

Distinguishing signatures of scalar leptoquarks at hadron and muon colliders

Priyotosh Bandyopadhyay^{a 1}, Anirban Karan^{a 2} and Rusa Mandal^{b 3}

^a *Indian Institute of Technology Hyderabad, Kandi, Sangareddy-502285, Telangana, India*

^b *Center for Particle Physics Siegen (CPPS), Theoretische Physik 1,
Universität Siegen, 57068 Siegen, Germany*

Abstract

While the hunt for new states beyond the standard model (SM) goes on for various well motivated theories, the leptoquarks are among the most appealing scenarios at recent times due to a series of tensions observed in B -meson decays. We consider two scalar leptoquarks, one being a singlet and the other a triplet under the electroweak gauge group, and respectively contributes to charged and neutral current B -meson decays. Focusing on the single production of these two scalar leptoquarks, we perform a PYTHIA-based simulation considering all the dominant SM backgrounds at the current and future setups of the large hadron collider. The final state consisting of a b and τ jets provides highest reach for the singlet leptoquark, whereas, for the triplet leptoquark $1 - \text{jet} + 2\mu + \cancel{p}_T$ topology is the most optimistic signature at the hadron colliders probing leptoquark couplings to fermions at $\mathcal{O}(10^{-1})$ value for a TeV mass range leptoquark. The invariant mass edge distribution is found to be instrumental in determination of the leptoquark mass scale at the LHC. Various distinguishing signatures are studied which can easily discriminate different components of the triplet leptoquark. Establishing a direct connection with the neutral current B -anomalies, we perform simulations for these leptoquarks at the proposed multi-TeV muon collider, where the background free environment can probe $\mathcal{O}(10^{-2})$ value of the leptoquark couplings to fermions for $\mathcal{O}(10)$ TeV leptoquark mass via $2 - \text{jet} + 2\mu$ signature.

¹Email: bpriyo@phy.iith.ac.in

²Email: kanirban@iith.ac.in

³Email: Rusa.Mandal@uni-siegen.de

Contents

1	Introduction	3
2	Framework	4
2.1	Theory and benchmark points	4
2.2	Set up for the LHC/FCC and muon colliders	6
3	S_1 at the LHC/FCC	6
3.1	Kinematic distributions and topologies	7
3.2	Final states including b and τ jets	10
3.2.1	$1b - \text{jet} + 1\tau - \text{jet} + 1\ell + \cancel{p}_T$	11
3.2.2	$1b - \text{jet} + 1\tau - \text{jet} + 2 - \text{jets} + \cancel{p}_T$	12
3.2.3	$1b - \text{jet} + \cancel{p}_T$	14
3.3	Final states including c and τ jets	14
3.3.1	$1c - \text{jet} + 1\tau - \text{jet} + \cancel{p}_T$	14
3.3.2	$1c - \text{jet} + 2\tau - \text{jet} + \cancel{p}_T$	15
3.4	Invariant mass edge distribution	16
4	S_3 at the LHC/FCC	18
4.1	Kinematic distributions and topologies	19
4.2	$S_3^{4/3}$ component of S_3 : $1 - \text{jet} + 2\mu + \cancel{p}_T$	24
4.3	$S_3^{2/3}$ component of S_3 : $1c - \text{jet} + \cancel{p}_T$	25
4.4	$S_3^{1/3}$ component of S_3	27
4.4.1	$1c - \text{jet} + 2\mu + \cancel{p}_T$	27
4.4.2	$1c - \text{jet} + 1\mu + \cancel{p}_T$	27
4.4.3	$1 - \text{jet} + \cancel{p}_T$	29
4.4.4	$1 - \text{jet} + 1\mu + \cancel{p}_T$	31
5	Lepton flavor violating decay signatures	32
6	Leptoquarks at muon collider	34
6.1	Kinematic distributions and topologies	37
6.2	$2 - \text{jet} + 2\mu$	39
6.3	$2c - \text{jet} + 2\mu$	40
6.4	$2b - \text{jet} + 2\mu$	41
6.5	$2b - \text{jet} + 4 - \text{jet} + 2\mu$	41
7	Comparison of results and reach at colliders	42
7.1	Discussion on S_1	43
7.2	Discussion on S_3	45
7.2.1	For the LHC/FCC	45
7.2.2	For a muon collider	47
8	Conclusion	48

1 Introduction

Leptoquarks among the most promising beyond the Standard Model (SM) candidates have been extensively searched at the experiments in past few years and the hunt is very much on at recent colliders. These color charged bosons couple to quark and leptons at the tree level and carry electromagnetic charge as well. Although the idea of quark-lepton unification was put forward in the 70's [1, 2], leptoquarks have drawn a significant attention recent days in order to explain the tensions observed in B -decays by several experimental collaborations [3–8].

Leptoquark can be pair or singly produced at the colliders and because of its strong interaction nature, pair production generally dominates at the LHC [9–14]. However the single production, which is governed by the model dependent Yukawa-type couplings, can also be significant in higher mass region [15, 16]. Such Yukawa-type couplings are directly related to the low energy processes like meson decays. Hence, at present when no signatures of these new particles have been found at the LHC, which in turn is regularly pushing the lower limit of the allowed masses upwards, it is important to study the single production in connection with the possible hints of new physics (NP) seen in B -decays.

In this paper, we focus on two scalar leptoquarks namely S_3 and S_1 having $(\bar{\mathbf{3}}, \mathbf{3}, 1/3)$ and $(\bar{\mathbf{3}}, \mathbf{1}, 1/3)$ quantum numbers, respectively, under the SM gauge group $(SU(3)_c, SU(2)_L, U(1)_Y)$. This choice is motivated with the possibility to address the discrepancies observed in either or both the $b \rightarrow s\mu\mu$ (neutral current (NC)) and $b \rightarrow c\tau\bar{\nu}$ (charged current (CC)) transitions [17–28]. Phenomenology of scalar leptoquarks at the colliders has been studied in literature with main emphasis on the pair production [29–50]. The distinct features of scalar and vector leptoquarks carrying all possible combinations of the SM gauge quantum numbers are explored at the lepton-photon collider [51], electron-proton collider [52] and at the LHC [53, 54] as well. The couplings to first generation of quarks and leptons are stringently constrained from Kaon and lepton physics [55–57] and the recent ATLAS searches performed with a center of mass energy of 13 TeV and an integrated luminosity of 139 fb^{-1} [58] exclude mass up to 1.8 TeV decaying into an electron and a quark. The limits are relatively weaker while looking for final states into third generation of fermions [59, 60].

The final state topologies studied in this work is directly related to the channels where certain tensions have been observed in B -decays and thus the phenomenology of S_1 leptoquark aims at modes with τ lepton and neutrinos in the final state whereas for S_3 leptoquark mostly muons and neutrinos are present. This provides very interesting and distinguishable signatures for the direct searches which can probe the most favored parameter space. Apart from the current setup of the Large Hadron Collider (LHC), this work also presents outcomes for the potential of the high luminosity LHC and the high energy LHC projects [61] to measure the properties of the considered leptoquarks. In view of the European Strategy Update for Particle Physics released its recommendation to investigate the technical and financial feasibility of a future hadron collider (FCC) at CERN with a center-of-mass energy of at least 100 TeV [62], we provide the analysis for such a setup as well.

Recently, there is a growing interest in the community for a multi-TeV muon collider which can succeed the LHC [63–66]. Due to less synchrotron radiation of muon compared to electron, no initial state QCD radiation, center of mass frame and significantly reduced background environment in contrast to hadron colliders, a muon collider has potential to look for new states beyond the SM [67–70]. The advantage is eminent for the NP mediators having direct connec-

tion to the $b \rightarrow s\mu\mu$ anomalies [71, 72]. Hence, in this article, we explore the phenomenology of S_3 leptoquark at muon collider as well. The pair production of leptoquark provides interesting signatures such as di-muon plus jets at muon collider which has spectacular sensitivity for the leptoquark coupling and mass parameters.

The rest of the paper is organized as follows. In section 2, we discuss the theoretical framework behind the choice of the benchmark scenarios (in subsection 2.1) and then specify the setup used for the phenomenological study at colliders (in subsection 2.2). We perform the LHC simulation for the single production of the scalar leptoquark S_1 in section 3; starting with the kinematic distributions (in 3.1) and then with two separate subsections (3.2 and 3.3) differing due to the flavor of the jets in the final states. The invariant mass edge distribution for S_1 is discussed in subsection 3.4. Similar analysis for the phenomenology at the current and future LHC for the scalar leptoquark S_3 is described in section 4. Several subsections are devoted to study the signatures arising from the different components of this electroweak triplet leptoquark and we separately analyze lepton flavor violating signatures in the decay for S_3 in section 5. We perform the simulation at a multi-TeV muon collider for the scalar leptoquarks in section 6. Finally, section 7 presents comparison of all the results for both of these leptoquarks highlighting the prospects at current and future colliders and our concluding remarks are mentioned in section 8.

2 Framework

In this section starting with the interaction Lagrangian of the two scalar leptoquarks, we obtain the benchmark scenarios which can explain any of the two types of tensions observed in neutral and charged current B -decays while being consistent with other data. Then we describe the basic set up used in our analysis to study the collider phenomenology at the LHC, FCC as well as at proposed multi-TeV muon collider.

2.1 Theory and benchmark points

We write the interaction Lagrangian for the two scalar leptoquarks $S_3(\bar{\mathbf{3}}, \mathbf{3}, 1/3)$ and $S_1(\bar{\mathbf{3}}, \mathbf{1}, 1/3)$ with the SM fermions as

$$\mathcal{L}_{\text{LQ}} = \overline{Q}^c i\tau_2 Y_{S_1}^{i\alpha} L^\alpha S_1 + \overline{u}_R^c Z_{S_1}^{i\alpha} \ell_R^\alpha S_1 + \overline{Q}^c Y_{S_3}^{i\alpha} i\tau_2 \boldsymbol{\tau} \cdot \mathbf{S}_3 L^\alpha, \quad (1)$$

where we denote the left-handed SM quark (lepton) doublets as Q (L), while u_R (d_R) and ℓ_R are the right-handed up (down)-type quark and lepton singlets, respectively. The notation $f^c \equiv \mathcal{C}\bar{f}^T$ indicates the charge-conjugated field of the fermion f . Here Y_{LQ} and Z_{LQ} are completely arbitrary Yukawa-type matrices in flavor space and τ_k , $k \in \{1, 2, 3\}$ are the Pauli matrices. Expanding the interaction terms in the mass-eigenstate basis we get

$$\begin{aligned} \mathcal{L}_{\text{LQ}} = & \left[\overline{u}_L^c (V^* Y_{S_1})^{ij} \ell_L^j - \overline{d}_L^c Y_{S_1}^{ij} \nu_L^j + \overline{u}_R^c Z_{S_1}^{ij} \ell_R^j \right] S_1 \\ & - \overline{d}_L^c Y_{S_3}^{ij} \nu_L^j S_3^{1/3} - \sqrt{2} \overline{d}_L^c Y_{S_3}^{ij} \ell_L^j S_3^{4/3} + \sqrt{2} \overline{u}_L^c (V^* Y_{S_3})^{ij} \nu_L^j S_3^{-2/3} - \overline{u}_L^c (V^* Y_{S_3})^{ij} \ell_L^j S_3^{1/3} \\ & + \text{h.c.} \end{aligned} \quad (2)$$

The transformation from the fermion interaction eigenstates to mass eigenstates is simply given by $u_L \rightarrow V^\dagger u_L$, where V is the quark Cabibbo-Kobayashi-Maskawa (CKM) matrix [73, 74] and we have neglected the unitary matrix in the neutrino sector. Note that, being a triplet under $SU(2)_L$, S_3 has three components differing in electric charges which are shown in the superscripts.

It is apparent from Equation 2 that at tree level, S_1 contributes to the $b \rightarrow c\tau\bar{\nu}$ transition, whereas, S_3 promotes $b \rightarrow s\mu\mu$ mode. The minimal set of non-zero couplings required for the above mentioned leptoquarks to explain either of the $b \rightarrow s\mu\mu$ and $b \rightarrow c\tau\bar{\nu}$ anomalies are summarized in Table 1. Here the contribution to CC mode is via the following effective Hamiltonian

$$\mathcal{H}_{\text{eff}}^{\text{CC}} = \frac{4G_F V_{cb}}{\sqrt{2}} [\mathcal{C}_L^S (\bar{c} P_L b) (\bar{\tau} P_L \nu) + \mathcal{C}_L^T (\bar{c} \sigma^{\mu\nu} P_L b) (\bar{\tau} \sigma_{\mu\nu} P_L \nu)] , \quad (3)$$

where

$$\mathcal{C}_L^S(M_{S_1}) = -4\mathcal{C}_L^T(M_{S_1}) = -\frac{v^2}{4M_{S_1}^2} \frac{1}{V_{cb}} Y_{S_1}^{33} Z_{S_1}^{*23} . \quad (4)$$

The ratios, defined as $R(D^{(*)}) \equiv \text{BR}(B \rightarrow D^{(*)}\tau\bar{\nu})/\text{BR}(B \rightarrow D^{(*)}\ell\bar{\nu})$, with $\ell = \{e, \mu\}$, can then be expressed as [75]

$$R(D)/R(D)_{\text{SM}} \approx 1 + 1.504 \text{Re} [\mathcal{C}_L^{S*}] + 1.171 \text{Re} [\mathcal{C}_L^{T*}] + 1.037|\mathcal{C}_L^S|^2 + 0.939|\mathcal{C}_L^T|^2 , \quad (5)$$

$$\mathcal{R}(D^*)/\mathcal{R}(D^*)_{\text{SM}} \approx 1 - 0.114 \text{Re} [\mathcal{C}_L^{S*}] - 5.130 \text{Re} [\mathcal{C}_L^{T*}] - 0.037|\mathcal{C}_L^S|^2 + 17.378|\mathcal{C}_L^T|^2 , \quad (6)$$

where the Wilson coefficients are evaluated at the m_b scale using renormalization group equations and neglecting electroweak contributions: $\mathcal{C}_L^{S(T)}(m_b) = 1.67(0.84) \times \mathcal{C}_L^{S(T)}(\Lambda = \mathcal{O}(\text{TeV}))$. The latest HFLAV average of $R(D^{(*)})$ data indicates 14% enhancements [8] compared to the SM predictions and two desired benchmark values are quoted in Table 1. We have checked that such benchmark points are allowed by the one-loop induced $Z \rightarrow \tau\tau$, $Z \rightarrow \nu\nu$ decays [76, 77] and B_s mixing bound [78]. Note that, S_1 also generates SM-like V-A operator, however, the required couplings to explain the $R(D^{(*)})$ anomalies are forbidden by $Z \rightarrow \tau\tau$ and B_s -mixing data.

In case of the NC anomalies we generate the following contribution to the effective Hamiltonian

$$\mathcal{H}_{\text{eff}}^{\text{NC}} = -\frac{4G_F}{\sqrt{2}} \frac{\alpha_{\text{EM}}}{4\pi} V_{td} V_{ts}^* [C_9^{\text{NP}} (\bar{s} \gamma^\mu P_L b) (\bar{\mu} \gamma_\mu \mu) + C_{10}^{\text{NP}} (\bar{s} \gamma^\mu P_L b) (\bar{\mu} \gamma_\mu \gamma_5 \mu)] , \quad (7)$$

where

$$C_9^{\text{NP}} = -C_{10}^{\text{NP}} = \frac{v^2}{M_{S_3}^2} \frac{\pi}{\alpha_{\text{EM}} V_{tb} V_{ts}^*} Y_{S_3}^{*32} Y_{S_3}^{22} . \quad (8)$$

The existing tensions observed in this mode can be achieved via $C_9^{\text{NP}} = -C_{10}^{\text{NP}} = -0.41_{-0.07}^{+0.07}$ [79] and such benchmark cases are shown in Table 1, which are allowed by the most constraining bounds arising from $Z \rightarrow \mu\mu$, $Z \rightarrow \nu\nu$ decays [76, 77] and B_s mixing [78]. The subsequent sections are devoted for detailed collider phenomenology studies of such benchmark scenarios for both S_1 and S_3 leptoquarks at the LHC/FCC and at a multi-TeV muon collider.

LQ	Mass (TeV)	NC	CC	Couplings	Benchmark points
S_1	1.5	✗	✓	$Y_{S_1}^{33} = 0.91, Z_{S_1}^{23} = -0.50$	BP1
	2.0			$Y_{S_1}^{33} = 1.10, Z_{S_1}^{23} = -0.74$	BP2
S_3	1.5			$Y_{S_3}^{22} = 0.50, Y_{S_3}^{32} = 0.003$	BP1
	2.0	✓	✗	$Y_{S_3}^{22} = 0.60, Y_{S_3}^{32} = 0.003$	BP2
	1.5			$Y_{S_3}^{22} = 0.008, Y_{S_3}^{32} = 0.20$	BP3

Table 1: The benchmark points defined with the minimal set of coupling values required for CC or NC anomalies for S_1 and S_3 leptoquarks. The symbol ‘✓’ (‘✗’) denotes agreement (disagreement) at $\pm 1\sigma$ level for the corresponding observables.

2.2 Set up for the LHC/FCC and muon colliders

In this subsection we summaries the kinematic cuts and definition of the collider set up that are used in simulations. Implementing the models in SARAH [80], model files are generated for CalcHEP [81]. The “.lhe” event files are then generated and interfaced with PYTHIA6.4.5 [82] for hadronization with initial state radiation (ISR) and final state radiation (FSR). The jet is formed using Fastjet-3.0.3 [83] with Cambridge/Aachen jet algorithm with a jet radius of 0.5. The additional basic cuts, written below, are also implemented.

- The calorimeter coverage is $|\eta| < 4.5$.
- The minimum jet transverse momentum $p_T = 20$ GeV and jets are ordered in p_T
- Leptons are selected with $p_T \geq 20$ GeV and $|\eta| < 2.5$.
- $\Delta R_{\ell j} \geq 0.4$ and $\Delta R_{jj} \geq 0.2$, where $\Delta R_{ij} = \sqrt{\Delta\eta_{ij}^2 + \Delta\Phi_{ij}^2}$ is the angle between the i -th and j -th particles, with $\Delta\Phi_{ij}$ is the difference of the azimuthal angle and $\Delta\eta_{ij}$ is the difference of the pseudo-rapidities.
- We demand that hadronic activity within a cone of $\Delta R = 0.3$ of the leptons should be $\leq 0.15 p_T^\ell$ GeV in the specified cone.
- In the case of $t\bar{t}$ and other SM background event generation we use a transverse momentum cut of > 1.2 TeV in order to avoid resonant SM background production. Such cut is also applied for the signal events to have a consistent setup and this does not affect the on-shell leptoquark production in the mass range (as shown in Table 1) chosen for this analysis.

3 S_1 at the LHC/FCC

In this section, we first start with the singlet leptoquark S_1 . In order to perform a collider analysis at the LHC/FCC, we choose the following set of center of mass energy (E_{CM}) values:

14 TeV, 30 TeV and 100 TeV and the dominant SM backgrounds are also taken into account accordingly. The benchmark points, quoted in Table 1, for two different S_1 masses namely, 1.5 TeV and 2.0 TeV are motivated from the explanation to CC anomalies seen in B -decays. Such parameter spaces are also allowed by the recent searches at the LHC [59, 60]. The main focus of this article is to probe the Yukawa-type coupling via single leptoquark production and the corresponding quark – gluon (g) fusion production modes can be seen from the leading order Feynman diagrams in Figure 1. The tree-level cross-sections for the $c - g$ and $b - g$ fusions are presented in Table 2 for three different center of mass energies of 14 TeV, 30 TeV and 100 TeV respectively, where NNPDF_lo_as_0130_qed [84] is used as parton distribution function, and $\sqrt{\hat{s}}$, the parton level center of mass energy is used as the renormalization/factorization scale. It can be seen that the $t - g$ fusion is not negligible at the E_{CM} of 30 TeV and 100 TeV due to enhanced parton distribution function contribution in NNPDF_lo_as_0130_qed [84]. Note that the K -factor for NLO single scalar leptoquark production in the high invariant mass region can at most be 1.5 [15] and for this analysis we neglect such scale factor. The leptoquarks produced from these mentioned channels will decay into $b\nu_\tau$, $t\tau$ and $c\tau$ final states with the branching ratios quoted in Table 3. Here we find that $b\nu_\tau$, $t\tau$ are the dominant modes which give rise to various final state topologies at discussed later in the subsections. Note that this minimal choice of parameter space forbids a decay to $c\mu$ mode which substantially reduces the SM backgrounds and can also nicely reconstruct the leptoquark invariant mass as found in [30]. The following subsections describe kinematical distributions and signal events and background events for several chosen topologies.

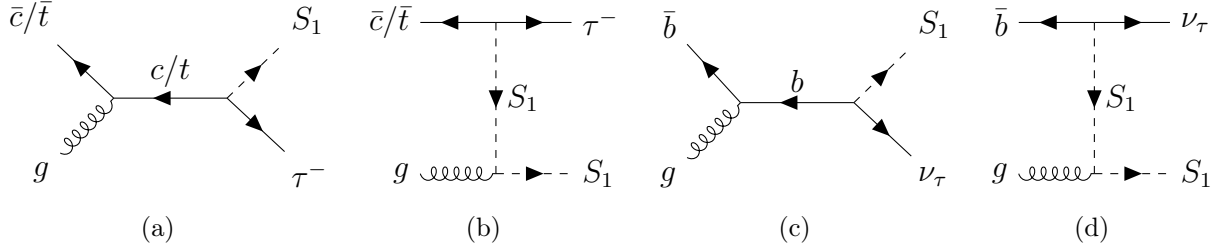


Figure 1: The tree level Feynman diagrams for $c/t - g$ and $b - g$ fusion producing S_1 leptoquark associated with a lepton.

3.1 Kinematic distributions and topologies

Before going into the details of the collider simulation let us have a look at the different differential distributions to motivate the advanced cuts which will be used later on to reduce the SM backgrounds. Depending on the decays of S_1 some final states may have more background than the rest. However, to reduce the light QCD-jet backgrounds we need more flavor tagging viz. b -jet and/or τ -jet. We first consider the production channel $c - g \rightarrow S_1\tau$ (shown in Figure 1(a)), where S_1 can further decay to either $b\nu$ or $c\tau$ states. Thus, final states involving b -, c - and τ -jets are possible and we discuss them separately. The dominant SM backgrounds arise from di-gauge bosons, viz. ZZ, WZ, WW , which contribute in the final states involving b - and τ -jets and the corresponding tagging efficiencies take care of such probabilities. Due to the large cross-section, similar situation can arise from $t\bar{t}$ as well; however, the demands of

Bench- mark Points	$\sigma(c - g \rightarrow S_1 \tau)$ in fb with E_{CM} in TeV			$\sigma(b - g \rightarrow S_1 \nu_\tau)$ in fb with E_{CM} in TeV			$\sigma(t - g \rightarrow S_1 \tau)$ in fb with E_{CM} in TeV		
	14 TeV	30 TeV	100 TeV	14 TeV	30 TeV	100 TeV	14 TeV	30 TeV	100 TeV
BP1	0.16	2.71	64.43	0.33	6.06	158.19	0.08	1.73	52.14
BP2	0.05	1.24	40.41	0.06	1.82	65.44	0.02	0.53	22.13

Table 2: The cross-sections at the LHC/FCC via $c - g$, $b - g$ and $t - g$ channels for the two benchmark points of S_1 leptoquark at three different center of mass energies of 14 TeV, 30 TeV and 100 TeV. We chose NNPDF_lo_as_0130_qed [84] as the parton distribution function and $\sqrt{\hat{s}}$ as renormalization/factorization scale.

Decay Modes	Branching fractions	
	BP1	BP2
$S_1 \rightarrow b \nu_\tau$	43.9	41.4
$S_1 \rightarrow t \tau$	42.8	40.4
$S_1 \rightarrow c \tau$	13.3	18.6

Table 3: Decay branching fractions in % for the allowed benchmark points of S_1 leptoquark.

only one b/c -jet, one or two τ -jet(s) and veto on light jets will definitely reduce the SM backgrounds to a negligible level. Interestingly the invariant mass-edge construction of $c - \tau$, which has a fall around the S_1 mass would further reduce the backgrounds. If we consider the decay of $S_1 \rightarrow t \tau$, the final states involving leptons are suppressed by branching fractions. For this analysis we considered b -jet tagging efficiency of $\sim 70\%$ via the secondary vertex reconstruction mechanism [85–87]. For τ -jet we reconstruct the hadronic one-prong (π^\pm) jet as τ -jet with momentum dependent efficiencies as shown in [88, 89].

In Figure 2(a) we show the jet multiplicity distribution for the signal of BP2 and the dominant SM background $t\bar{t}$ at the LHC with center of mass energy of 14 TeV. As a minimum transverse momentum cut for jets of greater than 1.2 TeV is applied, even $t\bar{t}$ peaks around 3, which is similar to the signal. Definitely the ISR and/or FSR increase(s) the jet multiplicity. In Figure 2(b) we depict the lepton multiplicity distribution both for BP2 and $t\bar{t}$ background at 14 TeV center of mass energy. It can be seen that for $t\bar{t}$ the main source of the leptons are from the W^\pm bosons which arise from the top quark decay. Similarly, in BP2 the hard charged lepton (e/μ) mainly comes from the decay to top quark which is produced from the S_1 decay. The source of the second lepton is mostly from the τ decay or the semileptonic decays of b quark. Hence our analysis mainly focuses on the mono-leptonic signature (e, μ), which is the hard one.

In Figure 3(a) we describe the jet p_T distributions of the p_T ordered jets coming from BP2 at 14 TeV center of mass energy. It is evident that the hardest jet p_T peaks around 900 GeV, which is

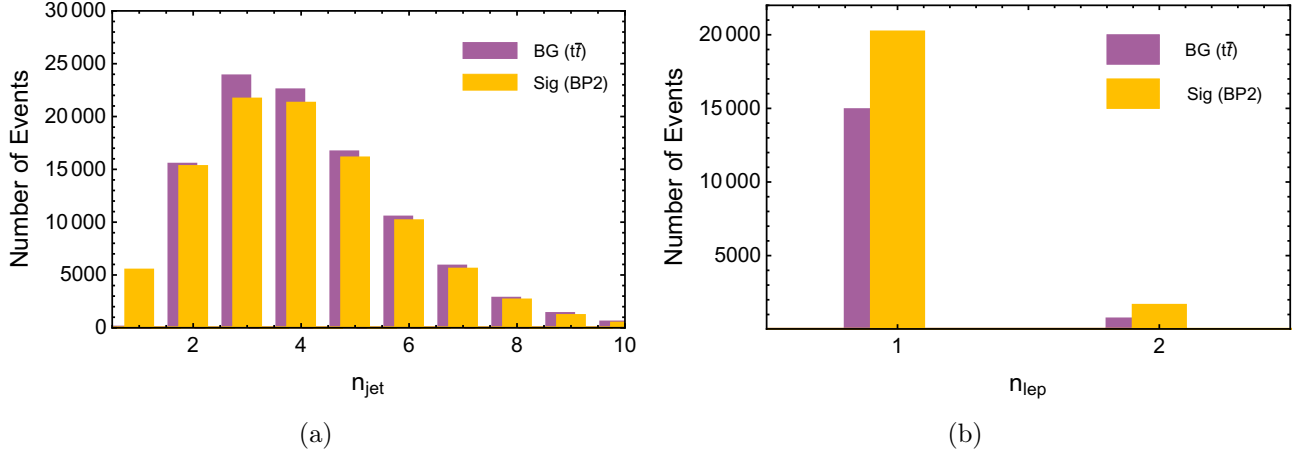


Figure 2: The jet (in (a)) and lepton (in (b)) multiplicity distributions for the BP2 and SM background $t\bar{t}$ at the LHC with center of mass energy of 14 TeV.

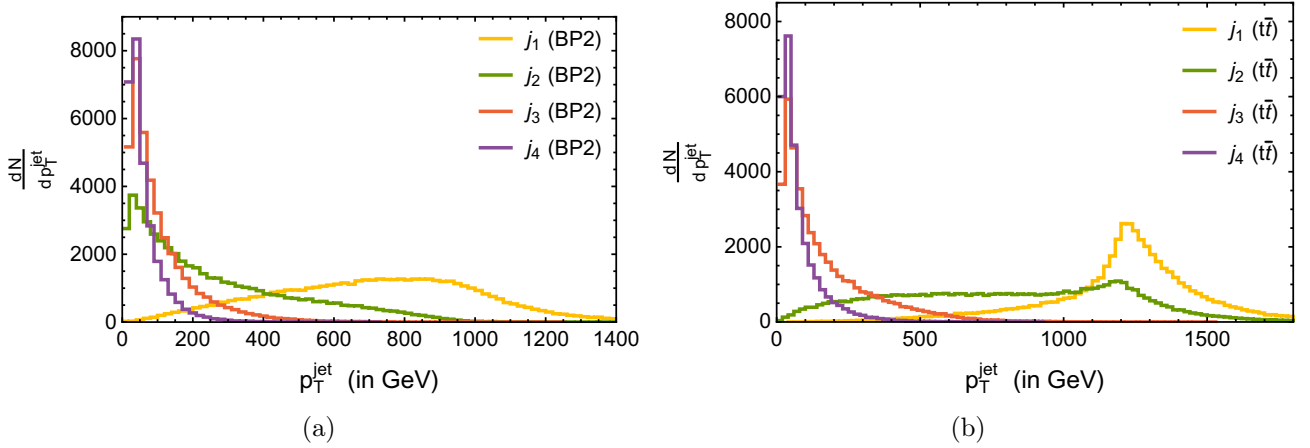


Figure 3: The jet p_T distributions for BP2 (in (a)) and the SM background $t\bar{t}$ (in (b)) at the LHC with center of mass energy of 14 TeV.

roughly at the half of leptoquark mass as expected. The second jet also has relatively larger tail. Figure 3(b) on the other hand shows the jet p_T distributions coming from the most dominant SM background $t\bar{t}$. In this case the hardest jet shows a peak at ~ 1.2 TeV as $p_T^{\text{min}} > 1.2$ TeV is used to generate the SM background events for the convergence of high p_T events relevant for the benchmark points (TeV mass leptoquarks) considered in our analysis.

We now move to the lepton p_T distributions as depicted in Figure 4(a). We see that the lepton coming from the signal is having higher p_T , whereas from $t\bar{t}$ the numbers are suppressed though the tail exists. Figure 4(b) shows the missing transverse momentum \cancel{p}_T distribution and it is evident that a large missing transverse momentum is observed which arises from the recoiled neutrino coming either at the production level for $b-g \rightarrow S_1 \nu_\tau$ or at the later stage from $c-g \rightarrow S_1(\rightarrow b\nu_\tau)\tau$. On the contrary, the missing transverse momentum \cancel{p}_T due to neutrinos in case of $t\bar{t}$ peaks near ~ 50 GeV. We apply missing transverse momentum cut $\cancel{p}_T > 200$ GeV, 500 GeV for the considered final states later in our analysis which reduce the SM backgrounds

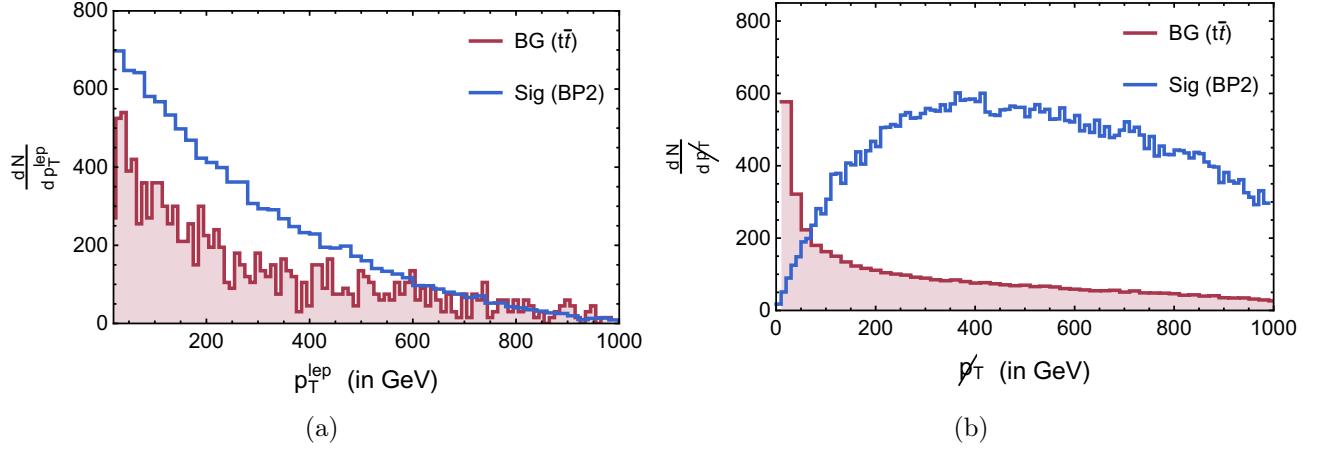


Figure 4: The lepton p_T (in (a)) and missing transverse momentum p_T^{miss} (in (b)) distributions for BP2 and the SM background $t\bar{t}$ at the LHC with center of mass energy of 14 TeV.

substantially.

3.2 Final states including b and τ jets

In this subsection we describe the final state topologies comprising b - and τ -jets for S_1 leptoquark production mainly via $c-g$ and $b-g$ fusions as well as with $t-g$ fusion which contributes at high energy. Once produced in association with τ -jet in $c-g$ fusion, the S_1 leptoquark further decays to $b\nu_\tau$, $t\tau$ states giving rise to the following topologies composed of at least one b - and τ -jet.

$$\begin{aligned} \text{BP1, BP2:} \quad c-g &\rightarrow S_1\tau, \\ &\rightarrow 1b\text{-jet} + 1\tau\text{-jet} + p_T^{\text{miss}}, \end{aligned} \quad (9)$$

$$\rightarrow 1b\text{-jet} + 2\tau\text{-jet} + 1\ell + p_T^{\text{miss}}, \quad (10)$$

$$\rightarrow 1b\text{-jet} + 2\tau\text{-jet} + 2\text{-jets}. \quad (11)$$

Similarly, $b-g \rightarrow S_1\nu_\tau$ can give rise to the following topologies with b - and τ -jet.

$$\begin{aligned} \text{BP1, BP2:} \quad b-g &\rightarrow S_1(\rightarrow b\nu_\tau, t\tau)\nu_\tau, \\ &\rightarrow 1b\text{-jet} + p_T^{\text{miss}}, \end{aligned} \quad (12)$$

$$\rightarrow 1b\text{-jet} + 1\tau\text{-jet} + 1\ell + p_T^{\text{miss}}, \quad (13)$$

$$\rightarrow 1b\text{-jet} + 1\tau\text{-jet} + 2\text{-jets} + p_T^{\text{miss}}. \quad (14)$$

Note that, unlike the previous case here we can have mono b -jet plus missing energy as an unique signature. The b -jet and c -jet tagging are followed with the corresponding efficiencies [85–87, 90]. From now onward, in the rest of the analysis, the light-jets are denoted as ‘jets’ ensuring no flavor tagging has been implemented. In the subsequent subsections we discuss all these final state signatures involving at least one b - and τ -jet at the LHC/FCC with three different center of mass energies namely 14 TeV, 30 TeV and 100 TeV.

E_{CM} in TeV	Mode	$1b - \text{jet} + 1\tau - \text{jet} + 1\ell + \cancel{p}_T$						
		Signal		Backgrounds				
		BP1	BP2	$t\bar{t}$	VV	VVV	$t\bar{t}V$	tZW
14	$c/t - g \rightarrow S_1 \tau$	3.34	1.38	1.60	0.00	0.00	0.00	0.00
	$b - g \rightarrow S_1 \nu$	0.58	0.17					
Total		3.92	1.55	1.60				
Significance		1.67	0.87					
$\mathcal{L}_{5\sigma}$ (fb $^{-1}$)		>>3000	>> 3000					
30	$c/t - g \rightarrow S_1 \tau$	83.46	47.04	37.42	2.05	0.01	0.11	0.03
	$b - g \rightarrow S_1 \nu$	13.75	4.67					
Total		97.21	51.71	39.62				
Significance		8.31	5.41					
$\mathcal{L}_{5\sigma}$ (fb $^{-1}$)		362.02	854.17					
100	$c/t - g \rightarrow S_1 \tau$	337.44	242.87	150.91	5.73	0.04	0.64	0.49
	$b - g \rightarrow S_1 \nu$	33.53	19.81					
Total		370.97	262.68	157.81				
Significance		16.13	12.80					
$\mathcal{L}_{5\sigma}$ (fb $^{-1}$)		9.61	15.26					

Table 4: The number of events for $1b - \text{jet} + 1\tau - \text{jet} + 1\ell + \cancel{p}_T$ final state for the benchmark points and dominant SM backgrounds at the LHC/FCC with the center of mass energies of 14 TeV, 30 TeV and 100 TeV where the integrated luminosity for the first two cases are at 1000 fb $^{-1}$ and 100 fb $^{-1}$ for 100 TeV. The required luminosities to achieve a 5 σ signal ($\mathcal{L}_{5\sigma}$) are also shown for all three cases.

3.2.1 $1b - \text{jet} + 1\tau - \text{jet} + 1\ell + \cancel{p}_T$

We tabulate the results for three different final states for which the signal significances are relatively on higher side. The event numbers at the center of mass energies of 14 TeV, 30 TeV and 100 TeV at the LHC/FCC with the respective integrated luminosities of 1000 fb $^{-1}$, 1000 fb $^{-1}$ and 100 fb $^{-1}$ are presented in Table 4 for the final state topology $1b - \text{jet} + 1\tau - \text{jet} + 1\ell + \cancel{p}_T$. It can be seen that $1b - \text{jet} + 1\tau - \text{jet} + 1\ell + \cancel{p}_T$ final state arises from both c/t -gluon fusion, where S_1 decays to $t\tau$ states. The top quark then provides the b -jet and the charged lepton via subsequent decays. When any of the two τ -jets is tagged we obtain the mentioned final state. Whereas for $b - g$ fusion we have only one τ -jet final state making the contribution significantly reduced for this case. The missing energy for the signal is relatively higher as can be seen from Figure 4(b) and we apply a cut of $\cancel{p}_T > 200$ GeV. The benchmark points are with masses 1.5, 2.0 TeV, so we apply a hardness cut of 1.2 TeV to reduce the background number of the events substantially, where the hardness cut $p_T^H = \Sigma(p_T^\ell + p_T^j + \cancel{p}_T)$, is the scalar sum of lepton, jet and missing transverse momentum. The first two hard jets p_T and the charged lepton p_T are demanded to be ≥ 200 GeV in order to reduce the SM backgrounds further as demonstrated in Figure 3. The

numbers presented in Table 4 at the 14 TeV center of mass energy with 1000 fb^{-1} luminosity are still not encouraging as a maximum of $\sim 1.7\sigma$ signal significance can be reached. Moving towards higher center of mass energy viz. 30 TeV in Table 4 give rise to the signal significances of 8.3σ and 5.4σ at 1000 fb^{-1} of integrated luminosity for BP1 and BP2, respectively. The results, in Table 4, quoted for 100 TeV center of mass energy are at the LHC/FCC are at an integrated luminosity of 100 fb^{-1} . The numbers are very encouraging with signal significances of $\sim 16\sigma$ and $\sim 13\sigma$ for BP1 and BP2, respectively. Note that in all cases $t\bar{t}$ remains the dominant SM background and some finite contributions also arises from the diboson states.

E_{CM} in TeV	Mode	$1b - \text{jet} + 1\tau - \text{jet} + 2 - \text{jets} + \cancel{p}_{\text{T}}$						
		Signal		Backgrounds				
		BP1	BP2	$t\bar{t}$	VV	VVV	$t\bar{t}V$	tZW
14	$c/t - g \rightarrow S_1 \tau$	21.62	7.44	66.17	0.00	0.00	0.01	0.00
	$b - g \rightarrow S_1 \nu$	16.81	4.22					
Total		38.43	11.66	66.18				
Significance		3.75	1.32					
$\mathcal{L}_{5\sigma} \text{ (fb}^{-1}\text{)}$		1777.78	>>3000					
30	$c/t - g \rightarrow S_1 \tau$	447.36	222.61	1773.95	22.62	0.04	0.80	0.13
	$b - g \rightarrow S_1 \nu$	359.86	146.48					
Total		807.22	369.09	1797.54				
Significance		15.82	7.93					
$\mathcal{L}_{5\sigma} \text{ (fb}^{-1}\text{)}$		99.89	397.55					
100	$c/t - g \rightarrow S_1 \tau$	1630.61	1005.55	7809.83	60.61	0.25	6.22	2.76
	$b - g \rightarrow S_1 \nu$	1013.87	556.94					
Total		2644.48	1562.49	7879.67				
Significance		25.78	16.08					
$\mathcal{L}_{5\sigma} \text{ (fb}^{-1}\text{)}$		3.76	9.67					

Table 5: The number of events for $1b - \text{jet} + 1\tau - \text{jet} + 2 - \text{light} - \text{jets} + \cancel{p}_{\text{T}}$ final state for the benchmark points and dominant SM backgrounds at the LHC/FCC with the center of mass energies of 14 TeV, 30 TeV and 100 TeV where the integrated luminosity for the first two cases are at 1000 fb^{-1} and 100 fb^{-1} for 100 TeV. The required luminosities to achieve a 5σ signal ($\mathcal{L}_{5\sigma}$) are also shown for all three cases.

3.2.2 $1b - \text{jet} + 1\tau - \text{jet} + 2 - \text{jets} + \cancel{p}_{\text{T}}$

Now here we consider the $1b - \text{jet} + 1\tau - \text{jet} + 2 - \text{jets} + \cancel{p}_{\text{T}}$ final state, which is almost similar to the previous decay topologies with only exception of the W^\pm , coming from the top quark, decays hadronically. Certainly, due to higher branching fraction in the hadronic mode, the event numbers increase substantially as compared to $1b - \text{jet} + 1\tau - \text{jet} + 1\ell + \cancel{p}_{\text{T}}$ in Table 4. We keep the cuts similar to the previous setup except for the two following demands: zero charged lepton

and total number of jets ≥ 4 in the final state. The number of events for the benchmark points as well as the dominant SM backgrounds are presented in Table 5. The results, presented at the LHC with center of mass energies of 14 TeV, 30 TeV are at an integrated luminosity of 1000 fb^{-1} , whereas, numbers for 100 TeV FCC are computed at an integrated luminosity of 100 fb^{-1} . We see that at 14 TeV the signal significance reaches 3.8σ for BP1 and 1.3σ for BP2. In this case, a 5σ signal strength for BP1 can be obtained with the larger data set of 1780 fb^{-1} integrated luminosity. The situation however improves at 30 TeV, where both the benchmark points cross 5σ of signal significance with very early data and have a maximum reach of 15.8σ for BP1 with 1000 fb^{-1} integrated luminosity. The results at 100 TeV LHC/FCC is very encouraging as even with 100 fb^{-1} integrated luminosity, we reach $\sim 26\sigma$ and 16σ of signal significance for BP1 and BP2, respectively. The $t\bar{t}$ remains the dominant background in this case as well and the effect of diboson is also quite significant.

E_{CM} in TeV	Mode	$1b - \text{jet} + p_{\text{T}}' > 500 \text{ GeV}$						
		Signal		Backgrounds				
		BP1	BP2	$t\bar{t}$	VV	VVV	$t\bar{t}V$	tZW
14	$c/t - g \rightarrow S_1 \tau$	1.34	0.42	32.12	0.00	0.00	0.00	0.00
	$b - g \rightarrow S_1 \nu$	17.66	4.15					
Total		19.00	4.57	32.12				
Significance		2.66	0.75					
$\mathcal{L}_{5\sigma} \text{ (fb}^{-1}\text{)}$		≥ 3000	$>> 3000$					
30	$c/t - g \rightarrow S_1 \tau$	15.98	7.84	368.66	29.69	0.02	0.15	0.02
	$b - g \rightarrow S_1 \nu$	270.24	97.67					
Total		286.22	105.51	398.55				
Significance		10.94	4.67					
$\mathcal{L}_{5\sigma} \text{ (fb}^{-1}\text{)}$		208.88	1146.32					
100	$c/t - g \rightarrow S_1 \tau$	41.80	24.92	588.57	23.14	0.09	0.55	0.21
	$b - g \rightarrow S_1 \nu$	555.02	263.83					
Total		596.82	288.75	612.56				
Significance		17.16	8.91					
$\mathcal{L}_{5\sigma} \text{ (fb}^{-1}\text{)}$		8.49	31.48					

Table 6: The number of events for $1b - \text{jet} + p'_T > 500 \text{ GeV}$ final state for the benchmark points and dominant SM backgrounds at the LHC/FCC with the center of mass energies of 14 TeV, 30 TeV and 100 TeV where the integrated luminosity for the first two cases are at 1000 fb^{-1} and 100 fb^{-1} for 100 TeV. The required luminosities to achieve a 5σ signal ($\mathcal{L}_{5\sigma}$) are also shown for all three cases.

3.2.3 $1b - \text{jet} + \cancel{p}_T$

In this case we consider the mode where S_1 decays to $b\nu_\tau$ states and this final state may only be composed of mono b -jet and missing energy, when S_1 being produced from $b - g$ fusion. Such a decay topology has a very unique signature, and we show the number of events and the SM backgrounds in Table 6 for the three center of mass energies at the LHC/FCC. where again the 14 TeV and 30 TeV results are for 1000 fb^{-1} integrated luminosity and the 100 TeV numbers are calculated for an integrated luminosity of 100 fb^{-1} . We have already inferred from the missing transverse momentum distribution in Figure 4, that either the recoiled or the neutrino arising from S_1 decay carries large energy, we impose a cut $\cancel{p}_T > 500 \text{ GeV}$ in order to reduce the SM backgrounds. The 14 TeV results show a signal significance of 2.7σ for BP1, whereas, BP2 fails to attain 1σ values. The 30 (100) TeV numbers depict a maximum of $\sim 11\sigma$ (17σ) and 5σ (9σ) signal significance for BP1 and BP2, respectively. In these two cases, a very early data can give rise to 5σ signal significance for both the benchmark points. Here $t\bar{t}$ still remains the dominant background.

3.3 Final states including c and τ jets

Now we aim to probe the other decay mode of S_1 namely to $c\tau$ states. With the two dominant production channels via $c - g$ and $b - g$ fusions, we look for topologies composed of at least one c -jet and τ -jet. The entire decay chain prompt us the following signals.

$$\begin{aligned} c - g &\rightarrow S_1\tau \\ &\rightarrow 1c - \text{jet} + 2\tau - \text{jet}, \end{aligned} \tag{15}$$

$$\begin{aligned} b - g &\rightarrow S_1\nu_\tau \\ &\rightarrow 1c - \text{jet} + 1\tau - \text{jet} + \cancel{p}_T. \end{aligned} \tag{16}$$

The c -jet tagging efficiency is taken around 56% with a mistagging of 12%, which is very conservative considering non-loose tagging mechanism [90]. Below we list the event numbers for the benchmark points (defined in Table 1) for the above mentioned final states along with the dominant SM backgrounds. We remind that as the considered leptoquark mass scale is assumed to be $\geq 1.5 \text{ TeV}$, we generate background events with $p_T > 1.2 \text{ TeV}$ for the better convergence of the background event number via simulation of PYTHIA [82]. The same momentum cut is also applied for the signal events of the benchmark points and does not affect the on-shell productions of the leptoquarks in the modes involved here.

3.3.1 $1c - \text{jet} + 1\tau - \text{jet} + \cancel{p}_T$

Table 7 presents the results for the $1c - \text{jet} + 1\tau - \text{jet} + \cancel{p}_T$ final state, where c -gluon, b -gluon as well as t -gluon contribute. Since the c -jet originates directly from the leptoquark decay we demand a relatively hard cut of $p_T > 200 \text{ GeV}$ for the c -jet. The τ -jet however, can either come directly from the production channel (for $c - g$ fusion) or from the leptoquark decay. Hence we also demand $p_T > 200 \text{ GeV}$ for the τ -jet. This almost implied that the first two p_T ordered jets are with $p_T > 200 \text{ GeV}$. The missing transverse momentum $\cancel{p}_T \geq 200 \text{ GeV}$ is demanded as well since the relatively boosted neutrino arise at the production level. The number of events listed for the benchmark points and dominant SM backgrounds in Table 7 are at an integrated

E_{CM} in TeV	Mode	$1c - \text{jet} + 1\tau - \text{jet} + \cancel{p}_{\text{T}}$						
		Signal		Backgrounds				
		BP1	BP2	$t\bar{t}$	VV	VVV	$t\bar{t}V$	tZW
14	$c/t - g \rightarrow S_1 \tau$	13.14	4.84	28.87	0.00	0.00	0.02	0.00
	$b - g \rightarrow S_1 \nu$	12.55	4.14					
Total		25.69	8.98	28.89				
Significance		3.48	1.46					
$\mathcal{L}_{5\sigma}$ (fb $^{-1}$)		2064.34	>>3000					
30	$c/t - g \rightarrow S_1 \tau$	315.62	153.26	672.38	11.52	0.11	1.84	0.11
	$b - g \rightarrow S_1 \nu$	259.40	128.75					
Total		575.02	282.01	685.96				
Significance		16.19	9.06					
$\mathcal{L}_{5\sigma}$ (fb $^{-1}$)		95.38	304.57					
100	$c/t - g \rightarrow S_1 \tau$	1253.23	783.41	2392.00	23.26	0.62	14.20	2.29
	$b - g \rightarrow S_1 \nu$	755.58	490.59					
Total		2008.81	1274.00	2432.37				
Significance		30.14	20.92					
$\mathcal{L}_{5\sigma}$ (fb $^{-1}$)		2.75	5.71					

Table 7: The number of events for $1c - \text{jet} + 1\tau - \text{jet} + \cancel{p}_T$ final state for the benchmark points and dominant SM backgrounds at the LHC/FCC, with center of mass energies of 14 TeV, 30 TeV and 100 TeV, where the integrated luminosity for the first two cases are at 1000 fb^{-1} and 100 fb^{-1} for 100 TeV. The required luminosities to achieve a 5σ signal ($\mathcal{L}_{5\sigma}$) are also shown for all three cases.

luminosity of 1000 fb^{-1} for 14 TeV and 30 TeV center of mass energies, and at 100 fb^{-1} for 100 TeV center of mass energy at the LHC/FCC. It is evident that for 14 TeV only BP1 crosses 3σ signal significance. However, for 30 TeV and 100 TeV the 5σ reach is possible with a very early data for both the benchmark points.

3.3.2 $1c - \text{jet} + 2\tau - \text{jet} + \cancel{p}_T$

In Table 8 we now tag one more τ -jet compared to the previous case and present $1c - \text{jet} + 2\tau - \text{jet} + \cancel{p}_T \geq 200 \text{ GeV}$ final states for the benchmark points and dominant SM backgrounds for the three different center of mass energies. Tagging one more τ -jet definitely reduces the events numbers both for the signal as well as for the backgrounds. We see a overall drop in the significance. Only for events at 30 TeV and 100 TeV collisions, we get a 5σ discovery reach. Nonetheless, this set up will help us in reconstructing the invariant mass edge of $c\tau$ which we discuss in the next in subsection 3.4.

E_{CM} in TeV	Mode	$1c - \text{jet} + 2\tau - \text{jet} + \cancel{p}_T$						
		Signal		Backgrounds				
		BP1	BP2	$t\bar{t}$	VV	VVV	$t\bar{t}V$	tZW
14	$c/t - g \rightarrow S_1 \tau$	2.49	1.12	0.98	0.00	0.00	0.00	0.00
	$b - g \rightarrow S_1 \nu$	0.33	0.11					
Total		2.82	1.23	0.98				
Significance		1.44	0.83					
$\mathcal{L}_{5\sigma}$ (fb $^{-1}$)		>>3000	>>3000					
30	$c/t - g \rightarrow S_1 \tau$	74.94	43.13	25.31	0.64	0.02	0.23	0.02
	$b - g \rightarrow S_1 \nu$	6.78	3.94					
Total		81.72	47.07	26.22				
Significance		7.87	5.50					
$\mathcal{L}_{5\sigma}$ (fb $^{-1}$)		403.64	826.45					
100	$c/t - g \rightarrow S_1 \tau$	347.22	238.14	71.68	1.26	0.10	2.11	0.37
	$b - g \rightarrow S_1 \nu$	22.62	13.73					
Total		369.84	251.87	75.52				
Significance		17.53	13.95					
$\mathcal{L}_{5\sigma}$ (fb $^{-1}$)		8.14	12.83					

Table 8: The number of events for $1c - \text{jet} + 2\tau - \text{jet} + \cancel{p}_T \geq 200$ GeV final state for the benchmark points and dominant SM backgrounds at the LHC/FCC with center of mass energies of 14 TeV, 30 TeV and 100 TeV where the integrated luminosity for the first two cases are at 1000 fb^{-1} and 100 fb^{-1} for 100 TeV. The required luminosities to achieve a 5σ signal ($\mathcal{L}_{5\sigma}$) are also shown for all three cases.

3.4 Invariant mass edge distribution

Ensuring the final states with excess events, we now look for invariant mass distributions for the resonance discovery of the leptoquark. The decay branching fractions quoted in Table 3 show that the leptoquark S_1 decays mostly to third generation fermions. It has been demonstrated in [30] that the third generation fermions give rise to a very rich final state; however, in the presence of a large number of jets, and specially the missing momentum from neutrino, the peaks are smeared. In case of a decay to $c\mu$ final state a very clear invariant mass peak can be constructed [30]. In this paper due the absence of such mode we demonstrate how invariant mass edge can be constructed, which is similar to a situation arises in supersymmetric theories with neutralino decays [91, 92].

As schematically shown in Figure 5(a), S_1 decays into a c -jet and a τ , which is detected as hadronic τ -jet [88, 89]. The neutrino in the final state contributes to missing energy but not to the τ -jet energy, which is identified as hadronic one-prong (π^\pm) jet. This results in a mass edge rather than a mass peak at the S_1 mass in the $c - \tau$ invariant mass distribution as given in

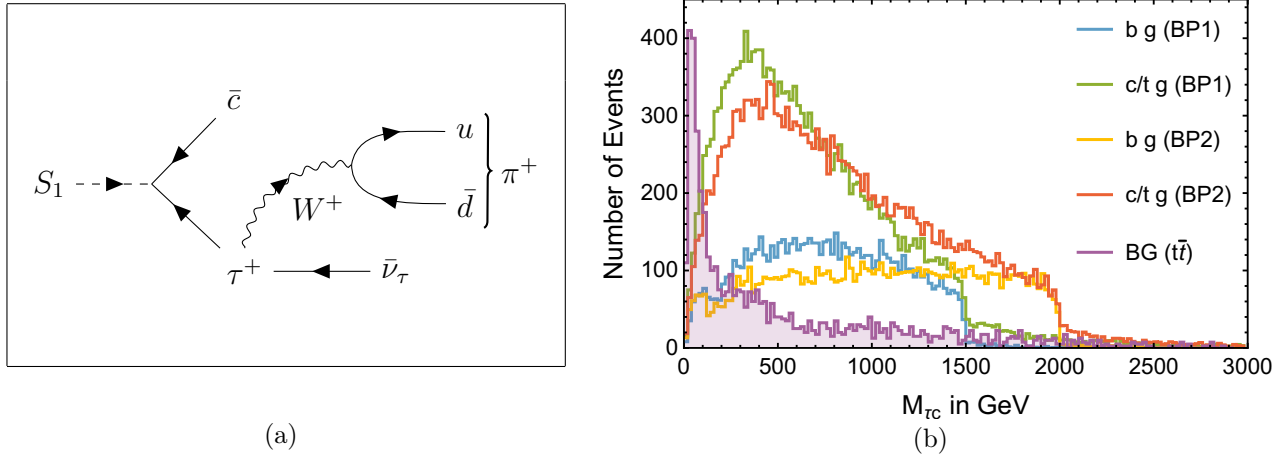


Figure 5: Panel (a) presents the Feynman diagram of $S_1 \rightarrow \bar{c} \tau \rightarrow \bar{c} \pi^+ \bar{\nu}_\tau$ and panel (b) shows the invariant mass edge of $m_{c\pi^+}^{\max}$ at the leptoquark mass M_{S_1} for the chosen scenarios BP1, BP2 and the SM background $t\bar{t}$ at 14 TeV center of mass energy at the LHC.

Equation 17.

$$\begin{aligned}
 m_{\pi c}^{\max} &= \frac{1}{m_\tau} [(m_{S_1}^2 - m_\tau^2)(m_\tau^2 - m_\nu^2)]^{1/2} \\
 &\simeq \frac{1}{m_\tau} (m_{S_1}^2 - m_\tau^2)^{1/2} m_\tau \simeq m_{S_1}.
 \end{aligned} \tag{17}$$

The mass edge can be calculated from a three-body decay S_1 , where the τ -jet accumulates the energy of the pion (π^\pm). This can be expressed in terms of the mass of the leptoquarks, mass of τ and the neutrino. As the leptoquark is at the TeV scale, from the collider perspective we can consider the last two particles as massless and this leaves us with the mass edge at $\sim m_{S_1}$ as shown in Equation 17. In Figure 5(b) we show the distributions at 14 TeV LHC for the two benchmark points BP1, BP2 and the dominant SM background $t\bar{t}$. It is clear that the invariant mass of c and τ (rather the π^+) $m_{c\pi^+}^{\max}$, gives mass edge at ~ 1.5 TeV and 2.0 TeV for the respective benchmark points, where the contributions are coming from all three production modes $b - g$ and $c/t - g$ fusions. The dominant SM background $t\bar{t}$ does not show any mass edge at these two regions.

We also present, in Table 9, the number of events for the interval $(m_{\pi c} < m_{\text{edge}}) - (m_{\pi c} \geq m_{\text{edge}})$ with reconstructed invariant mass of τ - and c - jets as $m_{\pi c}$ for the benchmark points and the total SM background at the LHC/FCC for three different center of mass energies. Similar to the previous analysis, the 14 TeV and 30 TeV results are for 1000 fb^{-1} integrated luminosity, whereas, 100 TeV numbers correspond to an integrated luminosity of 100 fb^{-1} . Here m_{edge} represents the mass-edge (or mass-wall) that we see for BP1 and BP2 in Figure 5(b) and thus a asymmetry around it is constructed by selecting events in the interval $(m_{\pi c} < m_{\text{edge}}) - (m_{\pi c} \geq m_{\text{edge}})$. Clearly, we see that except for the BP2 scenario with 14 TeV center of mass energy, all benchmark points cross 5σ signal significance. The background numbers in Table 9 includes contributions from all possible backgrounds such as $t\bar{t}$, VV , $VVV tWZ$ etc.

$(m_{\pi c} < m_{\text{edge}}) - (m_{\pi c} \geq m_{\text{edge}})$				
E_{CM}	Mode	BP1	BP2	Background
14 TeV	$c/t - g \rightarrow S_1 \tau$	81.46	23.92	75.18
	$b - g \rightarrow S_1 \nu$	51.98	11.00	
Total		133.44	34.92	
Significance		9.24	3.33	
$\mathcal{L}_{5\sigma} \text{ (fb}^{-1}\text{)}$		292.90	2257.25	
30 TeV	$c/t - g \rightarrow S_1 \tau$	1336.34	598.75	1527.44
	$b - g \rightarrow S_1 \nu$	947.27	326.50	
Total		2283.61	926.25	
Significance		37.00	18.70	
$\mathcal{L}_{5\sigma} \text{ (fb}^{-1}\text{)}$		18.27	71.50	
100 TeV	$c/t - g \rightarrow S_1 \tau$	3459.29	2146.94	5297.58
	$b - g \rightarrow S_1 \nu$	2390.10	1156.56	
Total		5849.39	3303.50	
Significance		55.40	35.62	
$\mathcal{L}_{5\sigma} \text{ (fb}^{-1}\text{)}$		0.82	2.00	

Table 9: the number of event combinations for $(m_{\pi c} < m_{\text{edge}}) - (m_{\pi c} \geq m_{\text{edge}})$ with reconstructed invariant mass of τ - and c - jets as $m_{\pi c}$ for the benchmark points and the total SM background at the LHC/FCC with center of mass energies of 14 TeV, 30 TeV and 100 TeV where the integrated luminosity for the first two cases are at 1000 fb^{-1} and the last one at 100 fb^{-1} . The required luminosities to achieve a 5σ signal ($\mathcal{L}_{5\sigma}$) are also shown for all three cases.

4 S_3 at the LHC/FCC

In this section we discuss the collider phenomenology of the S_3 leptoquark. Unlike S_1 , the $SU(2)_L$ triplet leptoquark S_3 has three components namely $S_3^{4/3}$, $S_3^{1/3}$, $S_3^{2/3}$ which are degenerate at the tree-level (see Equation 2). Finding distinguishable signatures for these different excitations can be challenging. In this article we illustrate how production modes vary depending on the leptoquark excitations. In Table 1 we present three benchmark scenarios corresponding to two different mass scales 1.5 TeV and 2 TeV for the leptoquark, and three different Yukawa-type coupling combinations. Note that, BP3 has largest $Y_{S_3}^{32}$ value which can lead to sizable interactions between the second and third generation of fermions. For this reason we separately discuss BP3 as lepton flavor violating (LFV) signatures in decay in section 5.

We list the Feynman diagrams for dominant single production processes of $S_3^{4/3}$, $S_3^{1/3}$ and $S_3^{2/3}$ via quark-gluon fusions in Figure 6. The cross-sections at the LHC for the center of mass energies of 14 TeV, 30 TeV and 100 TeV are listed in Table 10 for $s - g$ fusion and in Table 11 for $c - g$ fusion for the benchmark points BP1 and BP2. Here NNPDF_lo_as_0130_qed [84] has been used as parton distribution function where top quark is also included. The parton-level center of mass energy, i.e. $\sqrt{\hat{s}}$ is used as renormalization/factorization scale. It is interesting

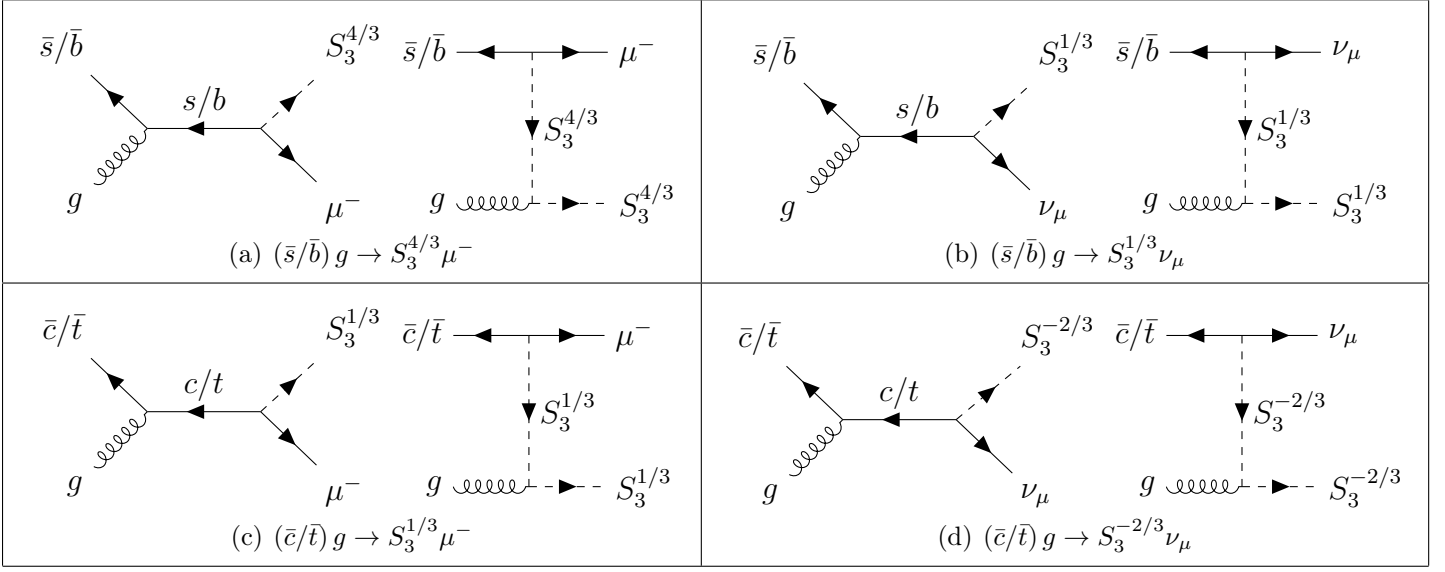


Figure 6: The tree level Feynman diagrams for $(s/b) - g$ and $(c/t) - g$ fusions producing different components of the leptoquark S_3 in association with a lepton.

to note that $S_3^{4/3}$ can only be produced via $s - g$ fusion, whereas, $S_3^{2/3}$ is produced through $c - g$ fusion for the chosen BP1 and BP2 scenarios. Due to different choices of couplings, in the case of BP3, the only production process for $S_3^{4/3}$ ($S_3^{2/3}$) is via $b - g$ ($t - g$) fusion and the results are depicted in Table 12 (Table 13). We notice that $S_3^{1/3}$ has contributions from both the production processes for the considered benchmark points. It is noteworthy that the production cross-section of $S_3^{1/3}$ in any particular fusion process is almost half of the production cross-section of $S_3^{4/3}$ and $S_3^{2/3}$ leptoquarks. This is due to the reason that the interaction vertex of $S_3^{4/3}$ and $S_3^{2/3}$ with quarks and leptons carry an additional $\sqrt{2}$ factor as can be observed from Equation 2. However, due to larger mass scale leptoquark (in TeV range), the cross-sections at 14 TeV center of mass energy is not quite promising and we need to depend on the collisions at 30 TeV and 100 TeV center of mass energies at the LHC/FCC.

Next, in Table 14 we list the decay branching fractions of the different excitations of S_3 for three benchmark points. We find that $S_3^{4/3}$ decays to $s\mu$ with 100% branching ratio for BP1 and BP2 and to $b\mu$ states with 100% branching ratio for BP3. Now for $S_3^{2/3}$, both $c\mu$ and $s\nu_\mu$ share 50% branching ratios for BP1 and BP2, whereas, for BP3 it decays to $t\mu$ and $b\nu_\mu$ states each with 50% branching fractions. The component $S_3^{1/3}$ decays completely (100% branching fraction) to $c\nu_\mu$ for BP1 and BP2, and for BP3 it decays to $t\nu_\mu$ states with 100% branching ratio.

4.1 Kinematic distributions and topologies

We compare various kinematic distributions for S_3 leptoquark with the dominant SM background arising from $t\bar{t}$ channel. For illustration we choose to discuss these distributions for BP1 at 100 TeV center of mass energy. The jet multiplicity distribution for the signal (in yellow) and $t\bar{t}$ background (in violet) are displayed in Figure 7(a) for the channel $cg \rightarrow S_3^{1/3}\mu$. All the four production channels for different components of S_3 , as shown in the Feynman diagrams in Figure 6, exhibit similar jet multiplicity distribution peaking around three, whereas, the SM

Benchmark	$\sigma(s - g \rightarrow S_3^{4/3} \mu)$ in fb			$\sigma(s - g \rightarrow S_3^{1/3} \nu_\mu)$ in fb		
	with center of mass energies in TeV			with center of mass energies in TeV		
Points	$E_{\text{CM}} = 14$	$E_{\text{CM}} = 30$	$E_{\text{CM}} = 100$	$E_{\text{CM}} = 14$	$E_{\text{CM}} = 30$	$E_{\text{CM}} = 100$
BP1	0.22	3.43	76.92	0.11	1.72	38.46
BP2	0.05	1.06	32.02	0.02	0.53	16.01

Table 10: The cross-sections (in fb) at the LHC via $s - g$ fusion of $S_3^{4/3}$ and $S_3^{1/3}$, for the two benchmark points, at three different center of mass energies 14 TeV, 30 TeV and 100 TeV, respectively. NNPDF_lo_as_0130_qed [84] is considered as the parton distribution function with $\sqrt{\hat{s}}$ as renormalization/factorization scale.

Benchmark	$\sigma(c - g \rightarrow S_3^{1/3} \mu)$ in fb			$\sigma(c - g \rightarrow S_3^{2/3} \nu_\mu)$ in fb		
	with center of mass energies in TeV			with center of mass energies in TeV		
Points	$E_{\text{CM}} = 14$	$E_{\text{CM}} = 30$	$E_{\text{CM}} = 100$	$E_{\text{CM}} = 14$	$E_{\text{CM}} = 30$	$E_{\text{CM}} = 100$
BP1	0.08	1.39	33.17	0.17	2.79	66.31
BP2	0.02	0.42	13.67	0.03	0.84	27.37

Table 11: The cross-sections (in fb) at the LHC via $c - g$ fusion of $S_3^{1/3}$ and $S_3^{2/3}$, for the two benchmark points, at three different center of mass energies 14 TeV, 30 TeV and 100 TeV. NNPDF_lo_as_0130_qed [84] is considered as the parton distribution function with $\sqrt{\hat{s}}$ as renormalization/factorization scale.

background $t\bar{t}$ peaks around six. At this point it is worth reminding that we have implemented a minimum transverse momentum cut of 1200 GeV to reduce the SM background substantially. Similarly, Figure 7(b) illustrates the lepton multiplicity distributions for signal and $t\bar{t}$ background for BP1 at 100 TeV center of mass energy. As discussed in previous section, the light charged leptons (e^\pm, μ^\pm) for $t\bar{t}$ essentially come from W^\pm bosons which are produced from the decay of the top quarks to bottom quarks. As the branching fraction of W^\pm to light charged leptons (e^\pm, μ^\pm) is only about 22%, most of the W^\pm decay hadronically producing no-lepton (dominant) and mono-lepton signatures for the background (in violet). In BP1, $S_3^{1/3}$ couples to both muon and ν_μ and thus, $c g \rightarrow S_3^{1/3} \mu$ (in blue) shows mono-lepton and di-lepton signatures, whereas, $s g \rightarrow S_3^{1/3} \nu_\mu$ (in green) shows non-leptonic and mono-leptonic signatures. Now, the component $S_3^{2/3}$ does not couple to any charged lepton displaying non-leptonic signature (in yellow) in the final state. Lastly, it is easy to see that the leptoquark $S_3^{4/3}$ couples to muon only, and hence

Benchmark	$\sigma(b - g \rightarrow S_3^{4/3} \mu)$ in fb			$\sigma(b - g \rightarrow S_3^{1/3} \nu_\mu)$ in fb		
	with center of mass energies in TeV			with center of mass energies in TeV		
Points	$E_{\text{CM}} = 14$	$E_{\text{CM}} = 30$	$E_{\text{CM}} = 100$	$E_{\text{CM}} = 14$	$E_{\text{CM}} = 30$	$E_{\text{CM}} = 100$
BP3	0.03	0.60	15.73	0.02	0.30	7.87

Table 12: The cross-sections (in fb) at the LHC via $b - g$ fusion of $S_3^{4/3}$ and $S_3^{1/3}$, for the benchmark point BP3, at three different center of mass energies 14 TeV, 30 TeV and 100 TeV. NNPDF_lo_as_0130_qed [84] is considered as parton distribution function with $\sqrt{\hat{s}}$ as renormalization/factorization scale.

Benchmark	$\sigma(t - g \rightarrow S_3^{1/3} \mu)$ in fb			$\sigma(t - g \rightarrow S_3^{2/3} \nu_\mu)$ in fb		
	with center of mass energies in TeV			with center of mass energies in TeV		
Points	$E_{\text{CM}} = 14$	$E_{\text{CM}} = 30$	$E_{\text{CM}} = 100$	$E_{\text{CM}} = 14$	$E_{\text{CM}} = 30$	$E_{\text{CM}} = 100$
BP3	0.004	0.09	2.60	0.01	0.17	5.18

Table 13: The cross-sections (in fb) at the LHC via $t - g$ fusion of $S_3^{4/3}$ and $S_3^{1/3}$, for the benchmark point BP3, at three different center of mass energies 14 TeV, 30 TeV and 100 TeV. NNPDF_lo_as_0130_qed [84] is considered as parton distribution function with $\sqrt{\hat{s}}$ as renormalization/factorization scale.

Decay	Branching ratios		Decay	Branching ratios
Modes	BP1	BP2	Modes	BP3
$S_3^{-4/3} \rightarrow s\mu$	100	100	$S_3^{-4/3} \rightarrow b\mu$	100
$S_3^{-1/3} \rightarrow c\mu$	50	50	$S_3^{-1/3} \rightarrow t\mu$	50
$S_3^{-1/3} \rightarrow s\nu_\mu$	50	50	$S_3^{-1/3} \rightarrow b\nu_\mu$	50
$S_3^{2/3} \rightarrow c\nu_\mu$	100	100	$S_3^{2/3} \rightarrow t\nu_\mu$	100

Table 14: The decay branching ratios (in percentage) of S_3 for the chosen benchmark points.

exhibiting mono-lepton and di-lepton signatures (in red).

In Figure 8, we portray the jet p_T distributions at 100 TeV center of mass energy. While

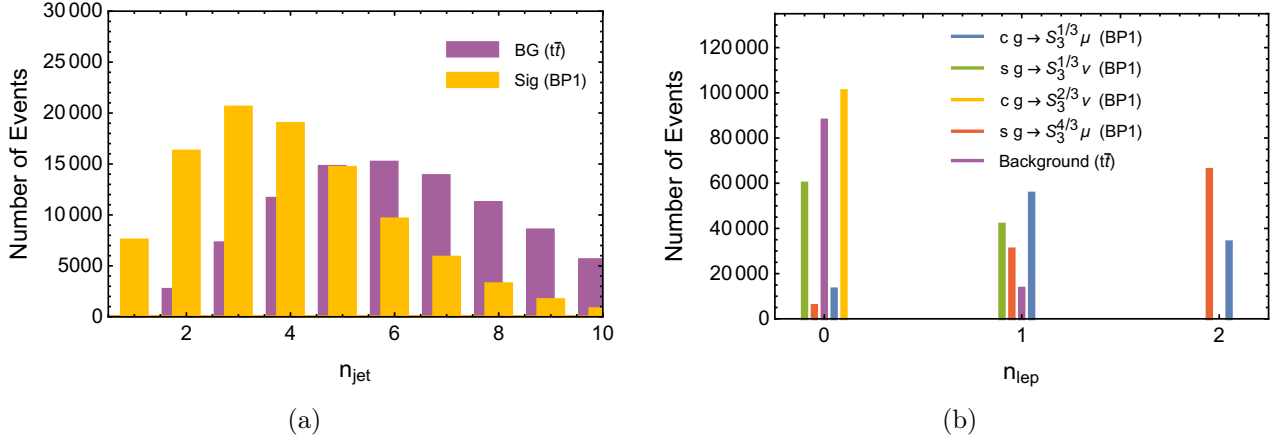


Figure 7: The jet (in (a)) and lepton (in (b)) multiplicity distributions of S_3 (for BP1) and the SM background $t\bar{t}$ at the LHC/FCC with the center of mass energy of 100 TeV.

Figure 8(a) represents the production channel $cg \rightarrow S_3^{1/3} \mu$ for BP1, all other components of S_3 provide similar distributions. Now, Figure 8(b) shows the dominant SM background $t\bar{t}$. Like S_1 leptoquark case, the hardest (in yellow) jet p_T in this case also peaks around half of the leptoquark mass (i.e. 750 GeV), as expected, and the second jet (in green) also shows relatively higher tail. All the four production channels for S_3 show similar jet p_T distributions. On the contrary, the jet p_T distributions from $t\bar{t}$ background reach their highest about 1200 GeV as a minimum transverse momentum cut of 1200 GeV has been implemented to generate the background converging at the high p_T events.

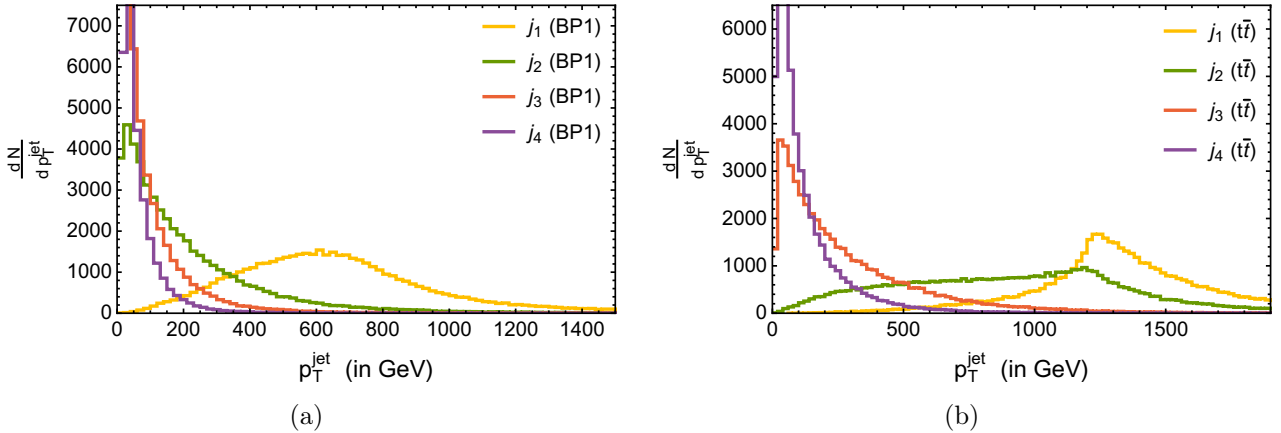


Figure 8: The jet p_T distributions of S_3 for BP1 (in (a)) and the SM background $t\bar{t}$ (in (b)) at the LHC/FCC with the center of mass energy of 100 TeV.

We show the transverse momentum distributions for light charged leptons (e^\pm, μ^\pm) for all the production channels of S_3 and $t\bar{t}$ background in Figure 9(a). As discussed above, the light charged leptons for $t\bar{t}$ background can only come from the W^\pm which produced from the decay of top quark, the lepton p_T distribution (in violet) exhibits a peak around the half mass of the W -boson and becomes insignificant for higher p_T^{lep} . The component $S_3^{2/3}$ does not couple to

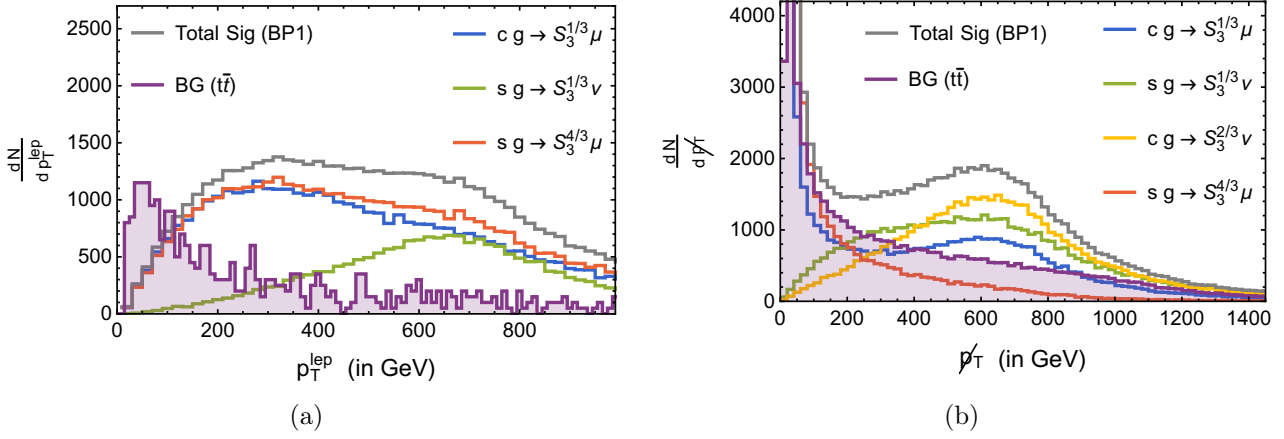


Figure 9: (a) distributions of lepton p_T and (b) missing p_T of S_3 (for BP1) with the SM background $t\bar{t}$ at the LHC with center of mass energy of 100 TeV.

charged leptons and hence does not contribute here. Now for the mode $sg \rightarrow S_3^{1/3}\nu$ (in green) as the charged lepton arises only from the decay of $S_3^{1/3}$, the lepton p_T distribution peaks around half the mass of leptoquark (i.e. 750 GeV). In the other two modes (in blue and red), muons are produced at two stages: firstly, during the production of the leptoquark, and secondly, during its decay. So, the distributions show quite similar behavior. However, as $S_3^{1/3}$ can decay to muon or neutrino, whereas, $S_3^{4/3}$ has channel only to muon (see Table 14). For this reason the p_T^{lep} distribution for $sg \rightarrow S_3^{4/3}\mu$ (in red) remains above the mode $cg \rightarrow S_3^{1/3}\mu$ (in blue). The grey curve depicts the total lepton p_T distribution for the components of S_3 leptoquark.

The missing p_T distributions for signals and dominant SM background have been presented in Figure 9(b). Like muons, the neutrinos in $t\bar{t}$ scenario also arise from leptonic decay of W^\pm , consequently the missing p_T distribution (in violet) peaks at lower p_T^{miss} and decreases gradually with a long tail. During the production and decay of $S_3^{4/3}$ (in red), no neutrino is involved showing a similar behavior of missing p_T distribution with a shorter tail. The production and decay of $S_3^{2/3}$ (in yellow) create two neutrinos, moving nearly opposite to each other with different momentum. However, the first neutrino at the production carries most of the missing transverse momentum and we observe a nice bell-shaped curve peaking around half of the leptoquark mass (i.e. 750 GeV). During the production of $S_3^{1/3}$ through $s-g$ fusion (in green), neutrino appears at production level and again, there is 50% probability for $S_3^{1/3}$ to decay to neutrino as well. Therefore, the p_T^{miss} distribution curve becomes a bit flat and resembles with in S_1 scenario. Finally, for $cg \rightarrow S_3^{1/3}\mu$ mode (in blue), when $S_3^{1/3}$ decays to muon the missing p_T shows a peak in low p_T^{miss} region similar to the $t\bar{t}$ background. Although, there is also a possibility for $S_3^{1/3}$ to decay to a neutrino exhibiting a local maximum about the half of the leptoquark mass. The grey curve depicts the total missing p_T distribution for the leptoquark S_3 .

We now focus on decay topologies arising from the single production channels for the two benchmark points BP1 and BP2. Our aim is to identify specific decay final states which can distinguish different components of the S_3 leptoquark. Due to particular gauge structure of the Lagrangian (in Equation 2), only $S_3^{4/3}$ and $S_3^{1/3}$ components of S_3 will be produced in $s-g$ fusion. Similarly, c -gluon fusion produces $S_3^{2/3}$ and $S_3^{1/3}$ components of S_3 only. However,

upon production, all these leptoquarks will decay to quarks and leptons. While $S_3^{4/3}$ and $S_3^{2/3}$ components decay to $s\mu$ and $c\nu_\mu$ respectively, $S_3^{1/3}$ decays to both the $s\nu_\mu$ and $c\mu$ topologies giving rise to the following final states:

$$\text{BP1, BP2:} \quad s - g \rightarrow S_3^{4/3}\mu \rightarrow 2\mu + 1 - \text{jet}, \quad (18)$$

$$s - g \rightarrow S_3^{1/3}\nu_\mu \rightarrow 1 - \text{jet} + \cancel{p}_T, \quad (19)$$

$$\rightarrow 1\mu + 1c - \text{jet} + \cancel{p}_T, \quad (20)$$

$$c - g \rightarrow S_3^{1/3}\mu \rightarrow 2\mu + 1c - \text{jet}, \quad (21)$$

$$\rightarrow 1\mu + 1 - \text{jet} + \cancel{p}_T, \quad (22)$$

$$c - g \rightarrow S_3^{2/3}\nu_\mu \rightarrow 1c - \text{jet} + \cancel{p}_T. \quad (23)$$

As already mentioned, here ‘jet’ implies light-jets unless the flavor is mentioned. We note that the complete decay chain of the leptoquark $S_3^{4/3}$ provides a unique final state of di-muon plus mono light jet. Similarly, we have unique signature for $S_3^{2/3}$ through the final state consisting of mono c -jet with missing energy. On the other hand, four different final states are possible involving the production of $S_3^{1/3}$ in quark-gluon fusion at LHC/FCC with BP1 and BP2. In the succeeding few subsections we describe the signal-background analyses for these six final states at center of mass energies of 14 TeV, 30 TeV and 100 TeV.

4.2 $S_3^{4/3}$ component of S_3 : $1 - \text{jet} + 2\mu + \cancel{p}_T$

As discussed earlier, leptoquark $S_3^{4/3}$ gets produced in association with muon from $s-g$ fusion via the Feynman diagram shown in Figure 6(a) and eventually decays into $s\mu$ with 100% branching fraction as presented in Table 14. This leads to the final state of mono-jet plus di-muon. The event numbers for the benchmark points BP1 and BP2 along with the dominant SM backgrounds for this final state are given in Table 15. The numbers are presented for three different center of mass energies viz. 14 TeV, 30 TeV and 100 TeV. The integrated luminosity are taken to be 1000 fb^{-1} for the first two and 100 fb^{-1} for the last one. Since the leptoquark masses in the considered benchmark points (BP1 and BP2) are taken to be 1.5 TeV and 2.0 TeV, a hardness cut of 1.2 TeV has also been implemented here to reduce the background. Both the hardest jet and lepton p_T cut are demanded to be $\geq 200 \text{ GeV}$. Moreover, as there is no neutrino involved in this final state, we put an upper limit on the missing energy as $\cancel{p}_T \leq 30 \text{ GeV}$. As expected, the dominant contribution to this mode comes from $sg \rightarrow S_3^{4/3}\mu$. Nevertheless, a small contribution arises from $cg \rightarrow S_3^{1/3}\mu$ as well, since it can also provide di-muon final state. On the other hand, $t\bar{t}$ and di-boson states remain the prepotent SM backgrounds. The signal significance achieved for this final state is very encouraging for all the three center of mass energies. In case of BP1, we reach the signal significances of 11.4σ , 44.7σ and 62.5σ respectively for the center of mass energies of 14 TeV, 30 TeV and 100 TeV. While integrated luminosity of $\sim 200 \text{ fb}^{-1}$ is required to reach 5σ significance at 14 TeV LHC, very early data of 13 fb^{-1} and 1 fb^{-1} are enough to gain the 5σ significance at 30 TeV and 100 TeV. In the case of BP2, due to lower production cross-section, the signal significances become 5.7σ , 26.1σ and 42.4σ for the three center of mass

\sqrt{s} in TeV	Fusion	Mode	$1 - \text{jet} + 2\mu + \cancel{p}_T$						
			Signal		Backgrounds				
			BP1	BP2	$t\bar{t}$	VV	VVV	$t\bar{t}V$	tZW
14	$s - g$	$S_3^{4/3}\mu$	116.07	31.02	3.40	0.00	0.00	0.00	0.00
		$S_3^{1/3}\nu$	0.00	0.00					
	$c - g$	$S_3^{1/3}\mu$	17.48	4.27					
		$S_3^{2/3}\nu$	0.00	0.00					
Total			133.55	35.29	3.40				
Significance			11.41	5.67					
$\mathcal{L}_{5\sigma}$ (fb $^{-1}$)			191.96	776.66					
30	$s - g$	$S_3^{4/3}\mu$	1824.64	688.31	63.83	69.55	0.11	0.43	0.05
		$S_3^{1/3}\nu$	0.00	0.00					
	$c - g$	$S_3^{1/3}\mu$	295.96	108.94					
		$S_3^{2/3}\nu$	0.00	0.00					
Total			2120.60	797.25	133.97				
Significance			44.66	26.13					
$\mathcal{L}_{5\sigma}$ (fb $^{-1}$)			12.53	36.63					
100	$s - g$	$S_3^{4/3}\mu$	3574.33	1776.17	196.19	110.45	0.57	3.26	0.91
		$S_3^{1/3}\nu$	0.00	0.00					
	$c - g$	$S_3^{1/3}\mu$	623.58	293.98					
		$S_3^{2/3}\nu$	0.00	0.00					
Total			4197.91	2070.15	311.38				
Significance			62.51	42.42					
$\mathcal{L}_{5\sigma}$ (fb $^{-1}$)			0.64	1.39					

Table 15: The number of events for $1 - \text{jet} + 2\mu + \cancel{p}_T \leq 30$ GeV final state (Equation 18) for the benchmark points and dominant SM backgrounds at the LHC/FCC with center of mass energy of 14 TeV, 30 TeV and 100 TeV at an integrated luminosity of 1000 fb $^{-1}$ for the first two and 100 fb $^{-1}$ for 100 TeV. The required luminosities to achieve a 5σ signal ($\mathcal{L}_{5\sigma}$) are also shown for all three cases.

energies, whereas, the required luminosities to achieve the 5σ significance are 777 fb $^{-1}$, 35 fb $^{-1}$ and 2 fb $^{-1}$, respectively.

4.3 $S_3^{2/3}$ component of S_3 : $1c - \text{jet} + \cancel{p}_T$

As we have pointed out earlier, $S_3^{2/3}$ can be produced only via $c - g$ fusion in association with a neutrino (Feynman diagram in Figure 6(d)) and then decays to $c\nu$ with 100% branching ratio. This leaves us with mono c -jet plus missing energy signature, which is very unique. The recoil of ν against $S_3^{2/3}$ leads to larger missing energy as already shown in Figure 9(b). In Table 16, the events for signal and the SM backgrounds are quoted again for the three different center

\sqrt{s} in TeV	Fusion	Mode	$1c - \text{jet} + \cancel{p}_T$						
			Signal		Backgrounds				
			BP1	BP2	$t\bar{t}$	VV	VVV	$t\bar{t}V$	tZW
14	$s - g$	$S_3^{4/3}\mu$	0.00	0.00	0.00	0.00	0.00	0.00	0.00
		$S_3^{1/3}\nu$	0.08	0.03					
	$c - g$	$S_3^{1/3}\mu$	0.00	0.00					
		$S_3^{2/3}\nu$	18.34	4.43					
Total			18.42	4.46	0.00				
Significance			4.29	2.11					
$\mathcal{L}_{5\sigma}$ (fb $^{-1}$)			1357.22	5605.38					
30	$s - g$	$S_3^{4/3}\mu$	0.00	0.00	0.00	1.13	0.00	0.00	0.00
		$S_3^{1/3}\nu$	1.41	0.53					
	$c - g$	$S_3^{1/3}\mu$	0.00	0.01					
		$S_3^{2/3}\nu$	244.28	87.42					
Total			245.69	87.96	1.13				
Significance			15.64	9.32					
$\mathcal{L}_{5\sigma}$ (fb $^{-1}$)			102.22	287.87					
100	$s - g$	$S_3^{4/3}\mu$	0.00	0.00	0.00	0.80	0.01	0.00	0.00
		$S_3^{1/3}\nu$	5.61	3.55					
	$c - g$	$S_3^{1/3}\mu$	0.13	0.11					
		$S_3^{2/3}\nu$	422.70	197.21					
Total			428.44	200.87	0.81				
Significance			20.67	14.14					
$\mathcal{L}_{5\sigma}$ (fb $^{-1}$)			5.85	12.50					

Table 16: The number of events for $1c - \text{jet} + \cancel{p}_T \geq 200$ GeV final state (Equation 23) for the benchmark points and dominant SM backgrounds at the LHC/FCC with center of mass energies of 14 TeV, 30 TeV and 100 TeV at an integrated luminosity of 1000 fb $^{-1}$ for the first two and 100 fb $^{-1}$ for 100 TeV. The required luminosities to achieve a 5σ signal ($\mathcal{L}_{5\sigma}$) are also shown for all three cases.

mass energies with the same choices for integrated luminosity as of all other cases discussed in this work. We put veto on the charged lepton as well as on the τ -jet, and demand only one c -jet with $p_T \geq 200$ GeV along with $\cancel{p}_T \geq 200$ GeV can be present. The results for 14 TeV are not very heartening especially for BP2, as the signal significance of 4.3σ and 2.1σ can be reached for BP1 and BP2, respectively at this center of mass energy. While a very high integrated luminosity is required for BP2 cases to reach 5σ limit, luminosity of ~ 1400 fb $^{-1}$ is enough for the same in case of BP1. Nonetheless, the situation improves quite a bit at 30 TeV where both the benchmark points reach 5σ signal significance at early stage of data collecting. Using 1000 fb $^{-1}$ of integrated luminosity one can achieve the signal significance of 15.6σ and 9.3σ for the two benchmark points respectively at this energy. Finally, the scenario looks very promising at

100 TeV collider because we can achieve 20.7σ and 14.1σ significances for the two corresponding benchmark points with only 100 fb^{-1} of integrated luminosity. It is interesting to mention that application of suitable cuts and vetoing τ and leptons make this mode almost free from SM backgrounds at all the three center of mass energies.

4.4 $S_3^{1/3}$ component of S_3

The component $S_3^{1/3}$ of S_3 leptoquark can be produced in association with a muon or a neutrino in $c-g$ and $s-g$ fusions. The produced leptoquark then disintegrates into either $c\mu$ or $s\nu_\mu$ with equal probability as shown in Table 14. Consequently, four different final states are possible in this scenario and we investigate them all sequentially.

4.4.1 $1c - \text{jet} + 2\mu + \cancel{p}_T$

In this case, we consider $S_3^{1/3}$ to be produced in accompany with a muon through $c-g$ fusion and eventually decays into a c -quark and a muon as shown in Equation 21. The signal-background analysis for this final state topology at LHC/FCC is illustrated in Table 17. Due to the absence of neutrinos in the entire decay chain ideally there should not be any missing energy and we impose the missing transverse momentum upper limit $\cancel{p}_T \leq 30\text{ GeV}$. We demand only one c -jet and one muon of the two having $p_T \geq 200\text{ GeV}$ along with τ -jet veto for the final state. Apart from the mentioned process, this final state gets very small contribution arising from $sg \rightarrow S_3^{4/3}\mu$ channel (discussed in subsection 4.2) as well, due to the miss tagging of light-jet as c -jet. Now, about the outcomes, the 14 TeV scenario is not very inspiring since significances of 3.4σ and 1.7σ can only be reached with 1000 fb^{-1} of integrated luminosity for the two respective benchmark points which implies the necessity of very high luminosity to attain 5σ reach. However, the situation improves with 30 TeV of center of mass energy where the signal significances of 14.2σ and 8.5σ can be obtained with 1000 fb^{-1} luminosity for BP1 and BP2 respectively which indicates requirement of only $\sim 130\text{ fb}^{-1}$ and $\sim 350\text{ fb}^{-1}$ integrated luminosities for 5σ reach. On the other hand, the results are very uplifting for 100 TeV center of mass energy as 21.4σ and 15.0σ of signal significances could be gained for BP1 and BP2, respectively, at 100 fb^{-1} of integrated luminosity only. Therefore significance of 5σ is reachable with very early data. It is important to mention that this final state is also almost free from the SM backgrounds except from small contributions arising from di-boson final states.

4.4.2 $1c - \text{jet} + 1\mu + \cancel{p}_T$

While considering the production of $S_3^{1/3}$ along with a neutrino via $s-g$ fusion and its disintegration into c -quark and a muon, the final state $1c - \text{jet} + 1\mu + \cancel{p}_T$ arises (see Equation 20). The demands are almost the same as the previous one except we have only one muon in this final state and due to the presence of a high energetic neutrino here, we put a lower bound on the missing transverse momentum as $\cancel{p}_T \geq 200\text{ GeV}$. The signal and background analysis at the LHC/FCC for this decay topology is presented in Table 18. With 14 TeV center of mass energy and 1000 fb^{-1} of luminosity, BP1 scenario provides a fair enough signal significance of 5.9σ implying $\sim 720\text{ fb}^{-1}$ of integrated luminosity is required for a 5σ significance. Although BP2 signal numbers cannot reach even 2.5σ significance. Compared to this, the situation is

\sqrt{s} in TeV	Fusion	Mode	$2\mu + 1c - \text{jet} + \cancel{p}_T$						
			Signal		Backgrounds				
			BP1	BP2	$t\bar{t}$	VV	VVV	$t\bar{t}V$	tZW
14	$s - g$	$S_3^{4/3}\mu$	0.78	0.24	0.00	0.00	0.00	0.00	0.00
		$S_3^{1/3}\nu$	0.00	0.00					
	$c - g$	$S_3^{1/3}\mu$	11.03	2.78					
		$S_3^{2/3}\nu$	0.00	0.00					
Total			11.81	3.02	0.00				
Significance			3.44	1.74					
$\mathcal{L}_{5\sigma}$ (fb $^{-1}$)			2116.85	8278.15					
30	$s - g$	$S_3^{4/3}\mu$	19.37	7.98	0.00	7.07	0.01	0.01	0.00
		$S_3^{1/3}\nu$	0.00	0.00					
	$c - g$	$S_3^{1/3}\mu$	189.51	71.22					
		$S_3^{2/3}\nu$	0.00	0.00					
Total			208.88	79.2	7.09				
Significance			14.21	8.53					
$\mathcal{L}_{5\sigma}$ (fb $^{-1}$)			123.75	343.61					
100	$s - g$	$S_3^{4/3}\mu$	61.10	32.09	0.00	0.57	0.03	0.12	0.05
		$S_3^{1/3}\nu$	0.00	0.00					
	$c - g$	$S_3^{1/3}\mu$	400.51	194.10					
		$S_3^{2/3}\nu$	0.00	0.00					
Total			461.61	226.19	0.77				
Significance			21.47	15.01					
$\mathcal{L}_{5\sigma}$ (fb $^{-1}$)			5.42	11.09					

Table 17: The number of events for $2\mu + 1c - \text{jet} + \cancel{p}_T \leq 30$ GeV final state (Equation 21) for the benchmark points and dominant SM backgrounds at the LHC/FCC with center of mass energy of 14 TeV, 30 TeV and 100 TeV at an integrated luminosity of 1000 fb $^{-1}$ for the first two and 100 fb $^{-1}$ for 100 TeV. The required luminosities to achieve a 5σ signal ($\mathcal{L}_{5\sigma}$) are also shown for all three cases.

quite better at 30 TeV center of mass energy as the signal significances of 23.8σ and 12.5σ can be obtained with 1000 fb $^{-1}$ integrated luminosity for BP1 and BP2, respectively, suggesting the 5σ reach for both the benchmark points with less than 200 fb $^{-1}$ of luminosity. Again, 100 TeV scenario is extremely cheering. Signal significances of 37.1σ and 23.7σ can be achieved for BP1 and BP2 respectively with 100 fb $^{-1}$ of integrated luminosity only. Therefore, very early data can provide significances of 5σ in this case. For this final state $cg \rightarrow S_3^{1/3}\mu$ also contributes significantly while there exists very small effect from $sg \rightarrow S_3^{4/3}\mu$ too. On the other hand, the SM background in this case is mainly governed by $t\bar{t}$ along with tiny contribution from di-boson channels.

\sqrt{s} in TeV	Fusion	Mode	$1\mu + 1c - \text{jet} + \cancel{p}_T$						
			Signal		Backgrounds				
			BP1	BP2	$t\bar{t}$	VV	VVV	$t\bar{t}V$	tZW
14	$s - g$	$S_3^{4/3}\mu$	0.27	0.08	7.68	0.00	0.00	0.00	0.00
		$S_3^{1/3}\nu$	37.82	9.40					
	$c - g$	$S_3^{1/3}\mu$	3.28	0.94					
		$S_3^{2/3}\nu$	0.00	0.00					
Total			41.37	10.42	7.68				
Significance			5.91	2.45					
$\mathcal{L}_{5\sigma}$ (fb $^{-1}$)			716.49	4167.57					
30	$s - g$	$S_3^{4/3}\mu$	9.27	3.98	159.57	14.70	0.11	0.45	0.06
		$S_3^{1/3}\nu$	611.56	221.92					
	$c - g$	$S_3^{1/3}\mu$	84.80	34.70					
		$S_3^{2/3}\nu$	0.00	0.00					
Total			705.63	260.60	174.89				
Significance			23.78	12.49					
$\mathcal{L}_{5\sigma}$ (fb $^{-1}$)			44.21	160.3					
100	$s - g$	$S_3^{4/3}\mu$	41.25	27.48	448.97	27.96	0.61	2.55	1.08
		$S_3^{1/3}\nu$	1367.82	666.88					
	$c - g$	$S_3^{1/3}\mu$	340.77	178.05					
		$S_3^{2/3}\nu$	0.00	0.00					
Total			1749.84	872.41	481.17				
Significance			37.05	23.71					
$\mathcal{L}_{5\sigma}$ (fb $^{-1}$)			1.82	4.45					

Table 18: The number of events for $1\mu + 1c - \text{jet} + \cancel{p}_T \geq 200$ GeV final state (Equation 20) for the benchmark points and dominant SM backgrounds at the LHC/FCC with center of mass energy of 14 TeV, 30 TeV and 100 TeV at an integrated luminosity of 1000 fb $^{-1}$ for the first two and 100 fb $^{-1}$ for 100 TeV. The required luminosities to achieve a 5σ signal ($\mathcal{L}_{5\sigma}$) are also shown for all three cases.

4.4.3 $1 - \text{jet} + \cancel{p}_T$

The final state of $1 - \text{jet} + \cancel{p}_T$ ensues from the production of $S_3^{1/3}$ in association with a neutrino via s -gluon fusion followed by its disintegration into a s -quark and a neutrino (see Equation 19). The signal and backgrounds for this final state are simulated in Table 19. Due to the fact that this final state incorporates two neutrinos, we have imposed a very high missing energy cut as $\cancel{p}_T \geq 500$ GeV. We also impose veto on charged leptons (e^\pm, μ^\pm) and τ -jet. The dominant SM background in this case comes from $t\bar{t}$, whereas, di-boson contributes sub-dominantly. On the contrary, the signal gets a huge contribution from the mode $cg \rightarrow S_3^{2/3}\nu$ as the c -jet mimics the light jet. A tiny contribution from $cg \rightarrow S_3^{1/3}\mu$ arises here as well. The simulation is performed

with the center of mass energies of 14 TeV, 30 TeV and 100 TeV at an integrated luminosity of 1000 fb^{-1} for the first two and 100 fb^{-1} for 100 TeV. The results for BP1 are very promising since signal significances of 6.9σ , 26.1σ and 40.2σ can be achieved with the above mentioned center of mass energies. This implies the requirements of 530 fb^{-1} , 37 fb^{-1} and 2 fb^{-1} of integrated luminosities only for a 5σ significance with the three collision energies. For BP2, with 14 TeV center of mass energy, the situation is not very heartening as only 2.1σ signal significance can be reached with 1000 fb^{-1} luminosity. However, like the previous cases, the scenarios become better at 30 TeV and 100 TeV, where significances of 11.3σ and 22.3σ can be obtained with luminosities of 1000 fb^{-1} and 100 fb^{-1} , respectively.

\sqrt{s} in TeV	Fusion	Mode	1 - jet+ \cancel{p}_T						
			Signal		Backgrounds				
			BP1	BP2	$t\bar{t}$	VV	VVV	$t\bar{t}V$	tZW
14	$s - g$	$S_3^{4/3}\mu$	0.07	0.02	155.65	0.02	0.00	0.01	0.00
		$S_3^{1/3}\nu$	31.66	8.33					
	$c - g$	$S_3^{1/3}\mu$	1.51	0.36					
		$S_3^{2/3}\nu$	79.66	19.77					
Total			112.9	28.48	155.68				
Significance			6.88	2.10					
$\mathcal{L}_{5\sigma}$ (fb $^{-1}$)			526.78	5675.17					
30	$s - g$	$S_3^{4/3}\mu$	1.51	0.87	1762.94	245.20	0.22	0.45	0.03
		$S_3^{1/3}\nu$	414.58	153.81					
	$c - g$	$S_3^{1/3}\mu$	28.85	9.40					
		$S_3^{2/3}\nu$	1111.06	407.98					
Total			1556.00	572.06	2008.84				
Significance			26.06	11.26					
$\mathcal{L}_{5\sigma}$ (fb $^{-1}$)			36.81	197.16					
100	$s - g$	$S_3^{4/3}\mu$	8.61	5.96	2237.31	245.20	0.80	1.66	0.33
		$S_3^{1/3}\nu$	737.86	355.10					
	$c - g$	$S_3^{1/3}\mu$	89.78	39.56					
		$S_3^{2/3}\nu$	2127.19	989.72					
Total			2963.44	1390.34	2485.30				
Significance			40.15	22.33					
$\mathcal{L}_{5\sigma}$ (fb $^{-1}$)			1.55	5.01					

Table 19: The number of events for $1 - \text{jet} + \cancel{p}_T \geq 500 \text{ GeV}$ final state (Equation 19) for the benchmark points and dominant SM backgrounds at the LHC/FCC with center of mass energy of 14 TeV, 30 TeV and 100 TeV at an integrated luminosity of 1000 fb^{-1} for the first two and 100 fb^{-1} for 100 TeV. The required luminosities to achieve a 5σ signal ($\mathcal{L}_{5\sigma}$) are also shown for all three cases.

4.4.4 $1 - \text{jet} + 1\mu + \cancel{p}_T$

\sqrt{s} in TeV	Fusion	Mode	$1 - \text{jet} + 1\mu + \cancel{p}_T$						
			Signal		Backgrounds				
			BP1	BP2	$t\bar{t}$	VV	VVV	$t\bar{t}V$	tZW
14	$s - g$	$S_3^{4/3}\mu$	23.55	7.18	15.93	0.02	0.00	0.00	0.00
		$S_3^{1/3}\nu$	64.38	15.27					
	$c - g$	$S_3^{1/3}\mu$	53.70	12.68					
		$S_3^{2/3}\nu$	0.00	0.00					
Total			141.63	35.13	15.95				
Significance			11.28	4.92					
$\mathcal{L}_{5\sigma}$ (fb $^{-1}$)			196.40	1034.75					
30	$s - g$	$S_3^{4/3}\mu$	511.42	216.42	332.34	586.11	0.48	0.16	0.05
		$S_3^{1/3}\nu$	1049.14	361.17					
	$c - g$	$S_3^{1/3}\mu$	972.80	352.44					
		$S_3^{2/3}\nu$	0.00	0.00					
Total			2533.36	930.03	919.14				
Significance			43.12	21.63					
$\mathcal{L}_{5\sigma}$ (fb $^{-1}$)			13.45	53.48					
100	$s - g$	$S_3^{4/3}\mu$	1936.37	1040.68	1173.36	992.48	2.47	0.84	0.91
		$S_3^{1/3}\nu$	2352.78	1083.01					
	$c - g$	$S_3^{1/3}\mu$	2473.30	1199.19					
		$S_3^{2/3}\nu$	0.00	0.00					
Total			6762.45	3322.88	2170.06				
Significance			71.55	44.84					
$\mathcal{L}_{5\sigma}$ (fb $^{-1}$)			0.49	1.24					

Table 20: The number of events for $1 - \text{jet} + 1\mu + \cancel{p}_T \geq 200$ GeV final state (Equation 22) for the benchmark points and dominant SM backgrounds at the LHC/FCC with center of mass energy of 14 TeV, 30 TeV and 100 TeV at an integrated luminosity of 1000 fb $^{-1}$ for the first two and 100 fb $^{-1}$ for 100 TeV. The required luminosities to achieve a 5σ signal ($\mathcal{L}_{5\sigma}$) are also shown for all three cases.

If the leptoquark $S_3^{1/3}$ is produced in c -gluon fusion associated with a muon and eventually decays to a s -quark and a neutrino, the final state $1 - \text{jet} + 1\mu + \cancel{p}_T$ appears as quoted in Equation 22. The event numbers along with different SM backgrounds have been shown in Table 20. As this final state involves one neutrino, a cut on missing transverse momentum is applied as $\cancel{p}_T \geq 200$ GeV along with $p_T \geq 200$ GeV for both the muon and the light-jet. Additionally, no b -jet and τ -jet are demanded to reduce the SM backgrounds. The di-boson and $t\bar{t}$ are the main SM backgrounds here. The results for both benchmark points for this final state are very encouraging. At 14 TeV, signal significances of 11.3σ and 4.9σ can be reached with

1000 fb⁻¹ of integrated luminosity inferring 200 fb⁻¹ and 1050 fb⁻¹ of luminosities to achieve 5 σ significance for BP1 and BP2, respectively. Similarly, signal significances of 43.2 σ and 21.6 σ at 30 TeV with 1000 fb⁻¹ luminosity and 71.6 σ and 44.8 σ at 100 TeV with luminosity of 100 fb⁻¹ can be attained for BP1 and BP2 respectively indicating that very low luminosity is required to achieve a 5 σ significance in this final state.

5 Lepton flavor violating decay signatures

In this section we discuss the signatures involving second and third generation fermion decays corresponding to the benchmark choice BP3 as quoted in Table 1. Due to different choice of coupling values, it can be seen from Table 14 that, we have different decay channels for the three components of S_3 as compared to the two previously investigated cases BP1 and BP2. In this case, S_3 is produced in association with a muon or a neutrino through via $b - g$ and $t - g$ fusions. Now, the components $S_3^{4/3}$ and $S_3^{2/3}$ decay to $b\mu$ and $t\nu_\mu$ states, respectively, whereas $S_3^{1/3}$ disintegrates into $t\mu$ and $b\nu_\mu$ with equal probabilities. The further decay of t -quark to a b -quark and a W -boson, and finally the W -boson decay modes will give rise to two jets or lepton plus missing energy signatures. The complete decay chain of these processes are as following.

$$\text{BP3:} \quad b - g \rightarrow S_3^{4/3} \mu \rightarrow 1b\text{-jet} + 2\mu, \quad (24)$$

$$b - g \rightarrow S_3^{1/3} \nu_\mu \rightarrow 1b\text{-jet} + 1\ell + 1\mu + \cancel{p}_T, \quad (25)$$

$$\rightarrow 1b - \text{jet} + 2 - \text{jet} + 1\mu + \cancel{p}_T, \quad (26)$$

$$\rightarrow 1b\text{-jet} + \cancel{p}_T, \quad (27)$$

$$t - g \rightarrow S_3^{1/3} \mu \rightarrow 1b - \text{jet} + 1\mu + \cancel{p}_T, \quad (28)$$

$$\rightarrow 1b - \text{jet} + 2 - \text{jet} + 2\mu, \quad (29)$$

$$\rightarrow 1b - \text{jet} + 1\ell + 2\mu + \cancel{p}_T, \quad (30)$$

$$t - g \rightarrow S_3^{2/3} \nu_\mu \rightarrow 1b - \text{jet} + 1\ell + \cancel{p}_T, \quad (31)$$

$$\rightarrow 1b - \text{jet} + 2 - \text{jet} + \cancel{p}_T. \quad (32)$$

We can see that, the production channel of $S_3^{4/3}$ provides unique signature as one b -jet plus di-muon. Whereas, for $S_3^{2/3}$ we get two final states depending on the decay of the top-quark, which arises from $S_3^{2/3}$. However, six different final states are possible for the two production processes of $S_3^{1/3}$. It is interesting to notice that unlike BP1 and BP2 scenarios of S_3 leptoquark, some final states for BP3 exhibit lepton flavor violating signatures (different lepton flavors in the final state) though the Lagrangian (in Equation 1) does not contain any explicit lepton flavor violating interaction.

Next, we analyze these final states at the LHC/FCC adopting the similar procedures described in previous sections at 14 TeV and 30 TeV center of mass energies with an integrated luminosity of 1000 fb⁻¹, also at 100 TeV collision with 100 fb⁻¹ of integrated luminosity. The signal numbers for all the above mentioned final states are very low for 14 TeV results and do not list them here. The events at 30 TeV and 100 TeV center of mass energies are noticeable, however, in most cases, they fail to attain a 5 σ signal strength within the proposed lifetime of

\sqrt{s} in TeV	Fusion	Mode	$1b - \text{jet} + 2 - \text{jet} + 2\mu + \cancel{p}_T$					
			Signal	Backgrounds				
			BP3	$t\bar{t}$	VV	VVV	$t\bar{t}V$	tZW
30	$b - g$	$S_3^{4/3}\mu$	35.88	0.00	1.56	0.00	0.00	0.00
		$S_3^{1/3}\nu$	0.00					
	$t - g$	$S_3^{1/3}\mu$	0.07					
		$S_3^{2/3}\nu$	0.00					
		Total						
Significance		5.87						
$\mathcal{L}_{5\sigma}$ (fb $^{-1}$)		725.59						
100	$b - g$	$S_3^{4/3}\mu$	59.70	0.00	0.46	0.00	0.01	0.00
		$S_3^{1/3}\nu$	0.02					
	$t - g$	$S_3^{1/3}\mu$	0.06					
		$S_3^{2/3}\nu$	0.00					
		Total						
Significance		7.70						
$\mathcal{L}_{5\sigma}$ (fb $^{-1}$)		42.15						

Table 21: The number of events for $1b - \text{jet} + 2 - \text{jet} + 2\mu + \cancel{p}_T \leq 30$ GeV for BP3 and dominant SM backgrounds at the LHC/FCC with center of mass energy of 30 TeV and 100 TeV at an integrated luminosity of 1000 fb $^{-1}$ and 100 fb $^{-1}$, respectively. The required luminosities to achieve a 5σ signal ($\mathcal{L}_{5\sigma}$) are also shown for both the cases.

LHC/FCC. The only encouraging scenario is the final state of $1b - \text{jet} + 2 - \text{jet} + 2\mu$, which according to the topologies quoted above arises from $S_3^{1/3}$ component (Equation 26). However, due to presence of initial state radiations and large production cross-section of $S_3^{4/3}$ (see Table 12), this component contributes dominantly via Equation 24. As no neutrino is present in this final state, we have applied a cut in the missing transverse momentum $\cancel{p}_T < 30$ GeV. The numbers for the signal and the SM background events are given in Table 21. The signal significances of 5.8σ at 30 TeV with 1000 fb $^{-1}$ integrated luminosity and 7.7σ at 100 TeV with luminosity of 100 fb $^{-1}$ can be attained for this benchmark point (BP3).

Instead of the demand of two muons in the final state, we have also investigated the situations with one muon, namely, the final states quoted in Equation 25, Equation 26 and Equation 28. Among these the scenario in Equation 25 is promising and the results are shown in Table 22. Here the $S_3^{1/3}$ is produced in association with a neutrino from $b - g$ fusion and decays into a neutrino and top quark that further decomposes semi-leptonically into a bottom quark, a light charged lepton and a neutrino. Since this final state contains two neutrinos, we impose a cut on missing transverse momentum as $\cancel{p}_T \geq 200$ GeV and also put veto on τ -jet as we only tag the electrons and the muons here. Though $\cancel{p}_T \geq 200$ cut reduces the contribution arising from $S_3^{4/3}$ compared to Table 21, but it is still the dominant contributor due to the large production cross-section. The dominant SM background in this case is $t\bar{t}$ and we obtain at the 30 TeV (100 TeV) center of mass energies with 1000fb $^{-1}$ (100fb $^{-1}$) of integrated luminosities the signal strengths

\sqrt{s} in TeV	Fusion	Mode	$1b - \text{jet} + 1\ell + 1\mu + \cancel{p}_T$					
			Signal	Backgrounds				
			BP3	$t\bar{t}$	VV	VVV	$t\bar{t}V$	tZW
30	$b - g$	$S_3^{4/3}\mu$	12.31	4.40	0.99	0.00	0.00	0.00
		$S_3^{1/3}\nu$	2.77					
	$t - g$	$S_3^{1/3}\mu$	0.21					
		$S_3^{2/3}\nu$	0.02					
		Total						
Significance		3.37						
$\mathcal{L}_{5\sigma}$ (fb $^{-1}$)		2207.80						
100	$b - g$	$S_3^{4/3}\mu$	22.77	3.77	0.69	0.01	0.01	0.00
		$S_3^{1/3}\nu$	5.64					
	$t - g$	$S_3^{1/3}\mu$	0.34					
		$S_3^{2/3}\nu$	0.03					
		Total						
Significance		4.99						
$\mathcal{L}_{5\sigma}$ (fb $^{-1}$)		100.39						

Table 22: The number of events for $1b - \text{jet} + 1\ell + 1\mu + \cancel{p}_T \geq 200$ GeV for BP3 and dominant SM backgrounds at the LHC/FCC with center of mass energy of 30 TeV and 100 TeV at an integrated luminosity of 1000 fb $^{-1}$ and 100 fb $^{-1}$, respectively. The required luminosities to achieve a 5σ signal ($\mathcal{L}_{5\sigma}$) are also shown for both the cases.

correspond to $\sim 3.3\sigma$ (5σ), respectively. However, for the two other topologies (Equation 26 and Equation 28) the signal numbers are quite low and the SM $t\bar{t}$ background numbers are significant which in turn reduces the signal strength considerably.

The situations further worsen in the topologies where no muon is present, which are Equation 27 for the $S_3^{1/3}$ component, and Equation 31 and Equation 32 for the $S_3^{2/3}$ part. In these cases, we do not obtain any significant signal strength due to the overwhelming SM background numbers. Hence we infer that unlike the previous cases with BP1 and BP2, here for BP3, different components of the S_3 leptoquark can not be discriminated via looking at distinguishable signatures.

6 Leptoquarks at muon collider

This section is devoted to explore leptoquarks at a proposed muon collider about which a growing interest is noticed at recent times. The reach of a multi-TeV muon collider is expected to be 90 ab $^{-1}$ with the center of mass energy of 30 TeV [93]. Due to the absence of initial state QCD radiation, reduced synchrotron radiation compared to electron collider and known center of mass frame, makes it a superior precision machine. In this section, we study the feasibility of producing leptoquarks in pair at muon collider. The initial setup and the kinematic cuts

remain the same as described in [subsection 2.2](#). For our choices of benchmark points, given in [Table 1](#), these production processes occur through the Feynman diagrams shown in [Figure 10](#). It is worthwhile to remind that the benchmark points are motivated from the tensions observed in B -decays, where the leptoquark S_1 couples only to third generation leptons aiming to reduce the $b \rightarrow c\tau\bar{\nu}$ discrepancy [8] and as a result, S_1 gets produced only through a photon and a Z^0 -boson mediated s -channel diagram ([Figure 10\(a\)](#)). While by construction of the benchmark points the leptoquark S_3 couples to muons contributing to $b \rightarrow s\mu\mu$ anomalies [3–7] and will be the prime candidate of our study at muon collider. Apart from the s -channel diagrams, S_3 can be produced via the quark mediated t -channel diagrams ([Figure 10\(b\)](#), [Figure 10\(c\)](#)) as well. The t -channel diagram for $S_3^{4/3}$ component of S_3 goes through a s -quark (BP1, BP2) or a b -quark (BP3), whereas for $S_3^{1/3}$ component a c -quark (BP1, BP2) or a t -quark (BP3) serves the purpose. It is noteworthy that $S_3^{2/3}$ does not couple to any charged lepton due to the structure of the interaction Lagrangian in [Equation 2](#), and hence it is produced at muon collider through the s -channel diagrams ([Figure 10\(a\)](#)) only.

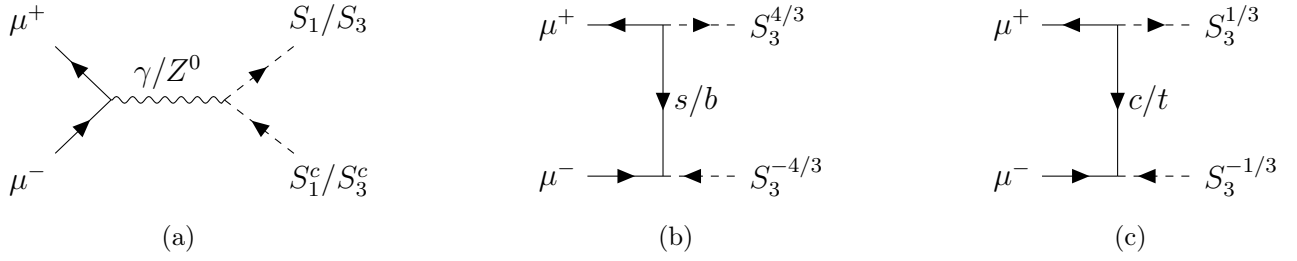


Figure 10: The tree-level Feynman diagrams for the pair production of S_1 and S_3 leptoquarks at a muon collider for the benchmark points specified in [Table 1](#).

As BP1 and BP2, quoted in [Table 1](#), differ mainly in the mass of the leptoquark, in this section we choose to present the results only for BP1 for simplicity, and BP3 as well. The variation of production cross-sections for S_3 leptoquark with the center of mass energy of the muon collider is presented in [Figure 11\(a\)](#) and [Figure 11\(b\)](#) for BP1 and BP3, respectively. The contributions arising from different components of S_3 leptoquark are separately presented with different color codes as specified in the plot legend. For BP1, $S_3^{4/3}$ shows prepotent effects while $S_3^{1/3}$ remains sub-dominant. In this case, the effects of t -channel diagrams are superior to the contributions from s -channel processes. However, for BP3, $S_3^{2/3}$ dominates at low center of mass energy and as energy starts increasing, $S_3^{4/3}$ becomes the main contributor to the total cross-section mostly via s -channel contribution. Due to smaller values of leptoquark Yukawa-type couplings in BP3, t -channel processes are suppressed compared to BP1. Note that the interference of t - and s -channel diagrams in [Figure 11\(c\)](#) introduces negative contribution, which are large at lower energies and are substantial even at higher energies. This keeps the cross-sections of $S_3^{4/3}$ and $S_3^{1/3}$ of the same order and results into a crossover of cross-sections for $S_3^{4/3}$ and $S_3^{2/3}$ around 6.5 TeV. It is easy to see from the two figures that the total production cross-section for S_3 in BP1 scenario is much higher than the BP3 case as the $Y_{S_3}^{22}$ coupling is significantly smaller in BP3 compared to BP1 (see [Table 1](#)). On the other hand, we have chosen the hardness cut of 1.2 TeV in our simulation, as discussed in [subsubsection 3.2.1](#), in such a way that the effects of s -channel processes could be neglected. Thus contributions from the $S_3^{2/3}$ in [Figure 11\(a\)](#) and

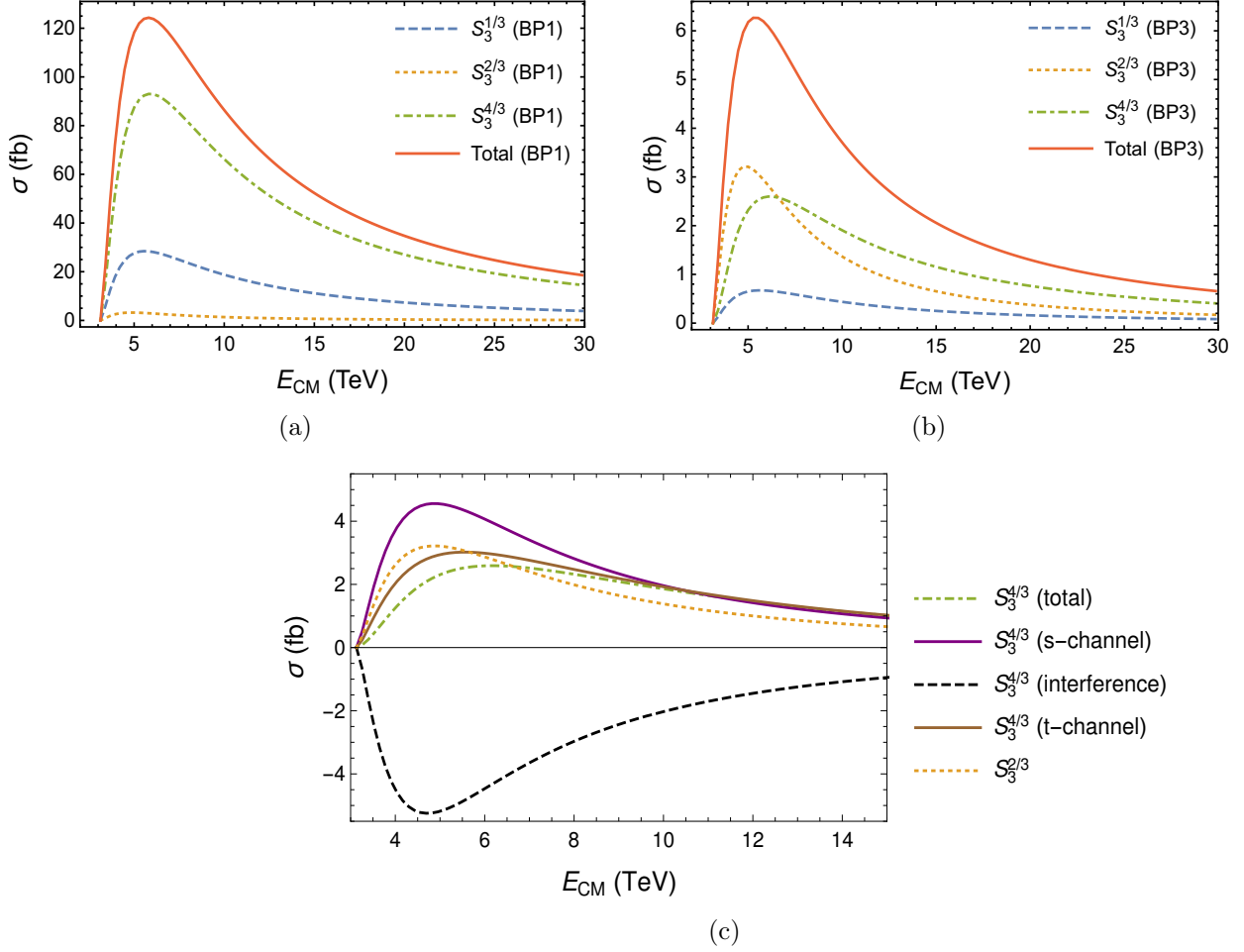


Figure 11: The variation of cross-sections for the pair production of S_3 leptoquark with the center of mass energy at a multi-TeV muon collider for BP1 (in (a)) and BP3 (in (b)). The blue (dashed), yellow (dotted) and green (dot-dashed) curves indicate individual contributions arising from $S_3^{1/3}$, $S_3^{2/3}$ and $S_3^{4/3}$ components of S_3 respectively, and the red (solid) line signifies the total production cross-section for S_3 leptoquark. The panel (c) zooms the BP3 case in the low energy region showing separately the s -channel (in purple solid), t -channel (in brown solid), interference of s - and t - channels (in black dashed) for $S_3^{4/3}$, as well as the total contributions of $S_3^{4/3}$ (in green dot-dashed) and $S_3^{2/3}$ (in yellow dotted) in the production cross-sections.

Figure 11(b) and similarly for S_1 leptoquark become negligible.

For our analysis, we pick two center of mass energies of 8 TeV and 30 TeV with the integrated luminosities of 1000 fb^{-1} and 10000 fb^{-1} , respectively. The cross-sections for pair production of different components of S_3 at these two center of mass energies are tabulated in Table 23. Interestingly enough, the cross-sections for pair production of $S_3^{1/3}$ are significantly smaller than that of $S_3^{4/3}$. Although apparently it seems that the ratio of these two cross-sections at some particular center of mass energy will be 1 : 4 due to the extra $\sqrt{2}$ factor in the interaction vertex of $S_3^{4/3}$ with quarks and leptons, the presence of s -channel diagrams and masses of t -channel propagators cause a deviation from this 1 : 4 ratio. On the other hand, the cross-sections for

$S_3^{4/3}$ and $S_3^{1/3}$ in BP3 case are around 40 times smaller than that in BP1 due to magnitude of $Y_{S_3}^{22}$ as mentioned previously. The production cross-section for $S_3^{2/3}$ at muon collider remains the same in BP1 and BP3 since this process involves s -channel gauge interactions only.

Bench- mark Points	$\sigma(\mu^+\mu^- \rightarrow S_3^{4/3} S_3^{-4/3})$		$\sigma(\mu^+\mu^- \rightarrow S_3^{1/3} S_3^{-1/3})$		$\sigma(\mu^+\mu^- \rightarrow S_3^{2/3} S_3^{-2/3})$	
	in fb with E_{CM} in TeV		in fb with E_{CM} in TeV		in fb with E_{CM} in TeV	
	8 TeV	30 TeV	8 TeV	30 TeV	8 TeV	30 TeV
BP1	80.74	14.75	23.36	3.95	1.94	0.17
BP3	2.32	0.41	0.55	0.08	1.94	0.17

Table 23: The cross-sections for pair production of S_3 at a multi-TeV muon collider for two different benchmark points BP1 and BP3 (specified in Table 1) at the center of mass energies of 8 TeV and 30 TeV. Here \sqrt{s} is used as the renormalization/factorization scale.

6.1 Kinematic distributions and topologies

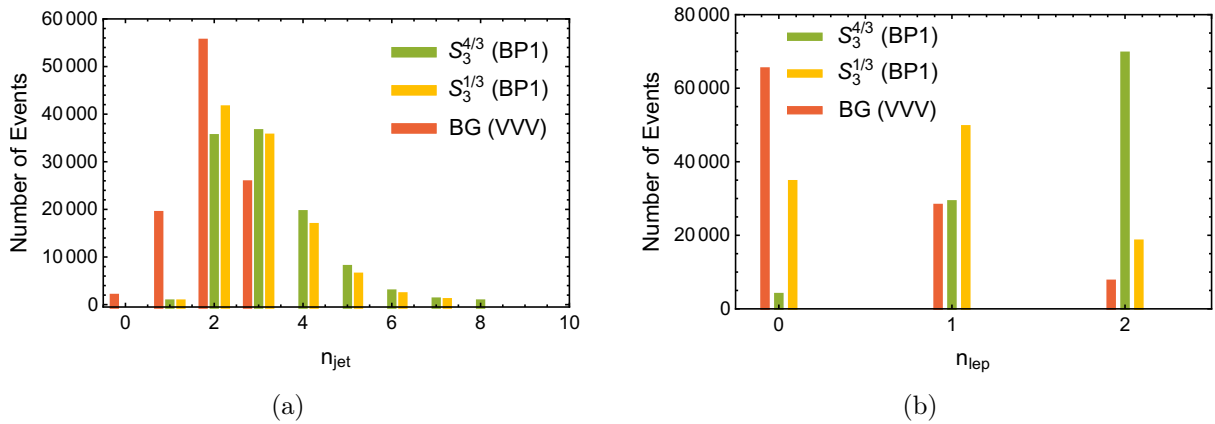


Figure 12: The jet (in (a)) and lepton (in (b)) multiplicity distributions for the pair production of $S_3^{4/3}$ and $S_3^{1/3}$ for BP1 along with the SM background from triple gauge boson at a muon collider with 8 TeV center of mass energy.

As discussed in the previous subsection 4.1, we start with the comparison of various kinematic distributions of the S_3 leptoquark and the dominant SM backgrounds at muon collider in order to understand the different interplay between hadron and muon collider. To demonstrate, we select BP1 scenario with 8 TeV of center of mass energy. At this point, it is interesting to mention that triple gauge boson modes act as dominant SM background for BP1 and it can be easily observed from the results quoted in Table 24 and Table 25 which will be discussed in the next subsection.

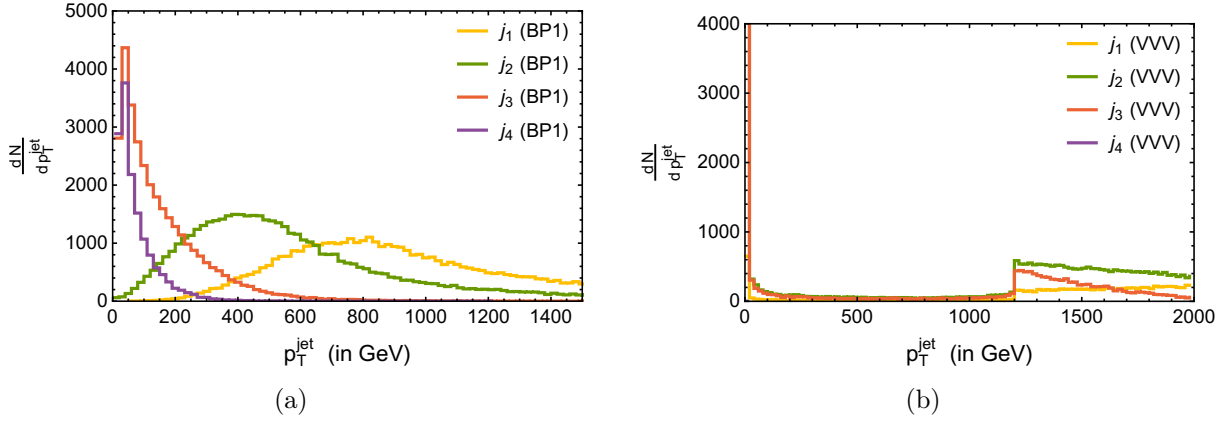


Figure 13: The jet p_T distribution of the pair production of $S_3^{4/3}$ in BP1 (in (a)) and the SM background from triple gauge boson (in (b)) at a muon collider with 8 TeV center of mass energy.

Figure 12(a) describes the jet multiplicity distribution for pair production of $S_3^{4/3}$ (in green) and $S_3^{1/3}$ (in yellow) along with the triple gauge boson background (in red). Although, all of these cases peak around two, it can be noticed that both the signals have significant amount of events for higher number of jets compared to the background. At this point, it should be remembered that a minimum transverse momentum cut of 1200 GeV has been imposed to reduce the SM background. In parallel, we have shown the lepton multiplicity distributions for $S_3^{4/3}$, $S_3^{1/3}$ and triple gauge boson background in Figure 12(b). As expected, $S_3^{4/3}$ displays peak with two muons while $S_3^{1/3}$ exhibits substantial contributions mainly to no-lepton and mono-lepton channels. This is due to the reason that $S_3^{4/3}$ component of S_3 in BP1 decays to $s\mu$ mode with 100% branching ratio (see Table 14), whereas, $S_3^{1/3}$ component decays to $c\mu$ and $s\nu$ with equal probability. However, the SM background coming from triple gauge bosons diminishes gradually with increase in lepton number at final state as the weak gauge bosons mostly decay into jets.

The jet transverse momentum distribution at 8 TeV muon collider has been depicted in Figure 13 where panel (a) represents pair production of $S_3^{4/3}$ and panel (b) signifies dominant SM background arising from the triple gauge bosons. The hardest jet (in yellow) in case of $S_3^{4/3}$ peaks around half of the leptoquark mass (i.e. 750 GeV), while second jet (in green) reaches its maximum about 400 GeV. The same pattern is also noticed for $S_3^{1/3}$ too. On the other hand, the jet p_T distributions for VVV background remain imperceptible till 1200 GeV and after that they gain some unavoidable contributions. This happens because of our implantation of 1200 GeV transverse momentum cut implemented in the event generation level.

The transverse momentum distributions for light charged leptons in the pair production channels of $S_3^{4/3}$ and $S_3^{1/3}$ along with the SM background arising from triple gauge boson have been depicted in Figure 14(a). Distributions for both the signals reach their maxima at 600 GeV, which is slightly lower than half of the leptoquark mass (i.e. 750 GeV). However, the distribution for the dominant SM background (in red) remains very flat. Similarly the missing transverse momentum p_T distributions are displayed in Figure 14(b). The distribution for VVV background remains very flat up to very high range of p_T . Whereas the p_T distributions for $S_3^{4/3}$ dies out very quickly as it does not involve any neutrino in its decay channel and $S_3^{1/3}$, which

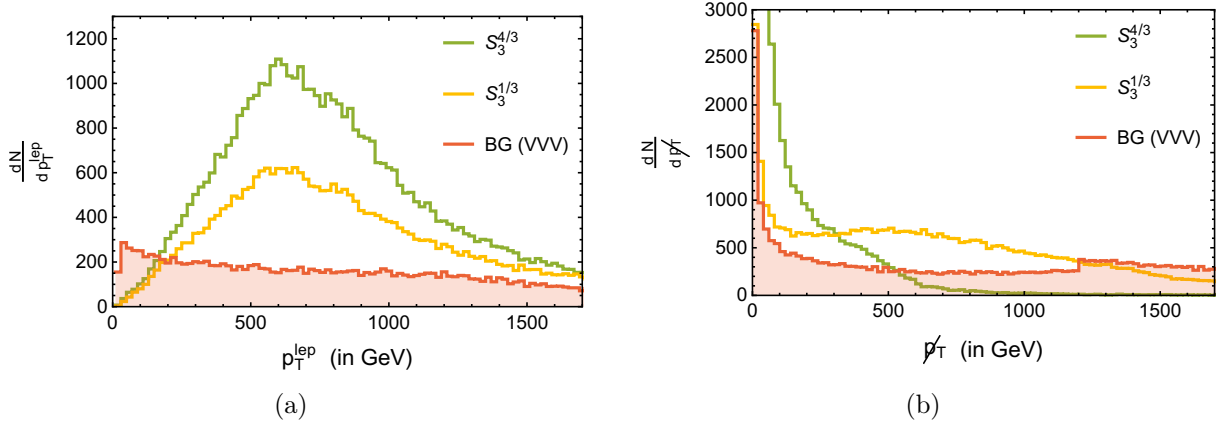


Figure 14: The lepton p_T (in (a)) and missing p_T (in (b)) distributions for $S_3^{4/3}$, $S_3^{1/3}$ and the SM background from triple gauge boson at a muon collider with center of mass energy of 8 TeV.

decays into $s\nu$ with 50% branching ratio, shows a relatively large tail.

$$\text{BP1 :} \quad \mu^+\mu^- \rightarrow S_3^{+4/3}S_3^{-4/3} \rightarrow 2\text{-jet} + 2\mu, \quad (33)$$

$$\mu^+\mu^- \rightarrow S_3^{+1/3}S_3^{-1/3} \rightarrow 2c\text{-jet} + 2\mu, \quad (34)$$

$$\text{BP3 :} \quad \mu^+\mu^- \rightarrow S_3^{+4/3}S_3^{-4/3} \rightarrow 2b\text{-jet} + 2\mu, \quad (35)$$

$$\mu^+\mu^- \rightarrow S_3^{+1/3}S_3^{-1/3} \rightarrow 2b\text{-jet} + 4\text{-jet} + 2\mu. \quad (36)$$

Now we proceed to study the detailed phenomenology of the two benchmark scenarios BP1 and BP3. After the pair production, $S_3^{4/3}$ decays into $s\mu$ ($b\mu$) with 100% branching fraction whereas, $S_3^{1/3}$ decays into $c\mu$ and $s\nu$ ($t\mu$ and $b\nu$) final states each with 50% branching fractions for BP1 (BP3) (see Table 14). Thus, for $S_3^{4/3}$, we have di-jet plus di-muon and two b -jets plus di-muon signals at the muon collider for BP1 and BP3, respectively. However, for $S_3^{1/3}$, several final states are plausible depending on its decay channels. Here, we only focus on those final states with no missing energy. It helps us to reduce the contamination from $S_3^{2/3}$ which despite of having a very low production cross-section, finally decays into final states with one neutrino for both the benchmark cases. Therefore for $S_3^{1/3}$, we consider two c -jets plus di-muon and two b -jets plus tetra-jet with di-muon topologies for BP1 and BP3, respectively. In the following few subsections we describe the simulated results for these four final states. We remind that we do not look for signals of $S_3^{2/3}$ in this section, as it gets produced through s -channel contributions only.

6.2 $2\text{-jet} + 2\mu$

This final state arises for $S_3^{4/3}$ in BP1 scenario (see Equation 33). The signal and background analyses for this final state at 8 TeV and 30 TeV center of mass energies with 1000 fb^{-1} and 10000 fb^{-1} of integrated luminosities are tabulated in Table 24. Triple gauge boson is the dominant background here, although tiny. The signal gets some contribution from $S_3^{1/3}$ mode, where the

c -jets are misidentified with light-jets. The results are very inspiring here since we can achieve $\sim 159\sigma$ of signal significance for BP1 at both of the center of mass energies with the specified luminosities. Therefore, significance of 5σ can be achieved at very early stage for both the center of mass energies. It is also interesting to notice that with the specified luminosities at both the center of mass energies one can attain more than 20σ significance for BP3 as well, in which the b -jet remains untagged. It is worth mentioning here that the reduction in production cross-sections at higher energy is compensated by our choice of enhanced luminosity (10000 fb^{-1}) at 30 TeV simulation. Thus the signal significance turns out to be very similar between 8 TeV and 30 TeV collisions for both the benchmark points.

\sqrt{s} in TeV	Mode	$2 - \text{jet} + 2\mu$					
		Signal		Backgrounds			
		BP1	BP3	$t\bar{t}$	VV	VVV	$t\bar{t}V$
8	$S_3^{4/3}$	23304.06	779.94	0.03	0.00	0.70	0.44
	$S_3^{1/3}$	1784.73	30.55				
Total		25088.79	810.49	1.17			
Significance		158.39	28.45				
$\mathcal{L}_{5\sigma}$ (fb $^{-1}$)		1.00	30.89				
30	$S_3^{4/3}$	23988.13	506.18	0.00	0.00	168.56	1.39
	$S_3^{1/3}$	1628.46	34.66				
Total		25616.59	540.84	169.95			
Significance		159.52	20.29				
$\mathcal{L}_{5\sigma}$ (fb $^{-1}$)		9.82	607.50				

Table 24: The number of events for 2-jet + 2μ final state (Equation 33) for the benchmark points and dominant SM backgrounds at a multi-TeV muon collider with the center of mass energy of 8 TeV and 30 TeV at an integrated luminosity of 1000 fb^{-1} and 10000 fb^{-1} , respectively. The required luminosities to achieve a 5σ signal ($\mathcal{L}_{5\sigma}$) are also shown for both the cases.

6.3 $2c$ -jet + 2μ

The final state $2c$ -jet + 2μ emerges for BP1 scenario when the $S_3^{1/3}$ component of S_3 is produced in pair and each of them decays into $c\mu$ states (in Equation 34). As mentioned earlier, this is not the only final state accessible at muon collider for $S_3^{1/3}$ with BP1, rather we choose this final state since it does not involve any missing energy. In addition to the preliminary cuts, b -jet veto is applied to suppress the fake signals arising from the mistagging of b -jets as c -jets. The results for this final state at the center of mass energies of 8 TeV and 30 TeV with the respective integrated luminosities of 1000 fb^{-1} and 10000 fb^{-1} are illustrated in Table 25. As the production cross-section of $S_3^{1/3}$ is considerably smaller than that of $S_3^{4/3}$, and furthermore the branching fraction of $S_3^{1/3}$ to $c\mu$ is only 50%, the signal numbers for this final state remain substantially low compared to the 2-jet + 2μ final state. Although, these number of events are large enough compared to the SM backgrounds which are negligible after imposition of suitable cuts, and thus

rendering $\sim 28\sigma$ signal significance at both the center of mass energies. Interestingly, it requires only 34 fb^{-1} and 302 fb^{-1} of integrated luminosities to obtain a 5σ signal significance at the two energies respectively. It is worth mentioning that BP3 scenario can also provide 5σ significance for this final state with luminosity less than 10000 fb^{-1} at both the center of mass energies.

\sqrt{s} in TeV	Mode	$2c - \text{jet} + 2\mu$					
		Signal		Backgrounds			
		BP1	BP3	$t\bar{t}$	VV	VVV	$t\bar{t}V$
8	$S_3^{4/3}$	0.81	4.29	0.00	0.00	0.03	0.00
	$S_3^{1/3}$	747.86	0.07				
Total		748.67	4.36	0.03			
Significance		27.36	2.08				
$\mathcal{L}_{5\sigma}$ (fb $^{-1}$)		33.39	5773.40				
30	$S_3^{4/3}$	2.95	28.85	0.00	0.00	4.32	0.00
	$S_3^{1/3}$	831.41	0.17				
Total		834.36	29.02	4.32			
Significance		28.81	5.03				
$\mathcal{L}_{5\sigma}$ (fb $^{-1}$)		301.18	9897.16				

Table 25: The number of events for $2c - \text{jet} + 2\mu$ final state (Equation 34) for the benchmark points and dominant SM backgrounds at a multi-TeV muon collider with the center of mass energy of 8 TeV and 30 TeV at an integrated luminosity of 1000 fb^{-1} and 10000 fb^{-1} , respectively. The required luminosities to achieve a 5σ signal ($\mathcal{L}_{5\sigma}$) are also shown for both the cases.

6.4 $2b - \text{jet} + 2\mu$

The final state of two b -jets with two muons emerges at muon collider when the $S_3^{4/3}$ component of S_3 leptoquark are produced in pair in BP3 scenario (Equation 35). The signal and background analyses for this final state at the similar previously specified setups for the center of mass energy and integrated luminosity are presented in Table 26. We see from Table 23 that the production cross-sections for both $S_3^{4/3}$ and $S_3^{1/3}$ in BP3 are significantly low compared to BP1 case, and hence the signal significance would also be reduced. However, as the SM backgrounds in this case are also negligible and thus this final state results are inspiring too. In fact, one can attain $\sim 26.5\sigma$ (20σ) significance at 8 TeV (30 TeV) energy with the specified integrated luminosity. It implies that less than 50 fb^{-1} (650 fb^{-1}) of luminosity is required to achieve the 5σ significance for this final state. Note that there is no significant signal events for this final state in BP1 scenario as apart from the demand of two b -jets, a limit on total number of light jets $n_j \leq 2$ is applied here.

6.5 $2b - \text{jet} + 4 - \text{jet} + 2\mu$

This particular final state appears if $S_3^{1/3}$ is produced at muon collider in pair in BP3 scenario and then both of them decay through $t\mu$ channel (Equation 36). The top quark would disinte-

\sqrt{s} in TeV	Mode	$2b - \text{jet} + 2\mu$					
		Signal		Backgrounds			
		BP1	BP3	$t\bar{t}$	VV	VVV	$t\bar{t}V$
8	$S_3^{4/3}$	0.00	680.58	0.00	0.00	0.00	0.31
	$S_3^{1/3}$	0.00	20.98				
Total		0.00	701.56	0.31			
Significance		0.00	26.48				
$\mathcal{L}_{5\sigma}$ (fb $^{-1}$)		—	35.65				
30	$S_3^{4/3}$	2.95	368.00	0.00	0.00	6.65	1.02
	$S_3^{1/3}$	0.00	25.17				
Total		2.95	393.17	7.67			
Significance		0.91	19.64				
$\mathcal{L}_{5\sigma}$ (fb $^{-1}$)		>>10000	648.26				

Table 26: The number of events for $2b - \text{jet} + 2\mu$ final state (Equation 35) for the benchmark points and dominant SM backgrounds at a multi-TeV muon collider with the center of mass energy of 8 TeV and 30 TeV at an integrated luminosity of 1000 fb $^{-1}$ and 10000 fb $^{-1}$, respectively. The required luminosities to achieve a 5σ signal ($\mathcal{L}_{5\sigma}$) are also shown for both the cases.

grate into a b -quark and a W -boson, and eventually the W -boson will produce two light jets. Thus, from the pair production of $S_3^{1/3}$, for BP3, we get $2b - \text{jet} + 4 - \text{jet} + 2\mu$ final state. However, this final state gets serious contribution from $S_3^{4/3}$ too. The results for this final state at 8 TeV and 30 TeV center of mass energies with the respective 1000 fb $^{-1}$ and 10000 fb $^{-1}$ of integrated luminosities are quoted in Table 27. At 8 TeV center of mass energy with 1000fb $^{-1}$ of data one can reach $\sim 15\sigma$ of signal significance for BP3 indicating a need of ~ 110 fb $^{-1}$ of integrated luminosity to achieve a 5σ signal significance. Surprisingly, one can reach 10.9σ signal significance at the same energy with 1000 fb $^{-1}$ of data for BP1 case as well contributing through the $2 - \text{jet} + 2\mu$ channel. However, the results for 30 TeV is not heartening at all since we need integrated luminosity of more than 10000 fb $^{-1}$ to achieve 5σ significance.

7 Comparison of results and reach at colliders

In order to identify the best outcomes of the previous sections and their implications in future searches at the colliders, in this section we explore the particular regions in the NP parameter space where more than 5σ signal significance can be reached with the specific choices of center of mass energy and integrated luminosity. For this purpose we select those final states which have very small model background (i.e. the contamination from other production channels). Then we observe the variation of significance with the parameters of the NP model, namely, the mass of the leptoquark and its couplings with quarks and leptons keeping the center of mass energy and integrated luminosity fixed at the specific choices. It should be noted that though the SM backgrounds remain unaltered for any specific center of mass energy and luminosity, the model background (along with signal) varies with the change in the parameters of the NP model.

\sqrt{s} in TeV	Mode	$2b - \text{jet} + 4 - \text{jet} + 2\mu$					
		Signal		Backgrounds			
		BP1	BP3	$t\bar{t}$	VV	VVV	$t\bar{t}V$
8	$S_3^{4/3}$	112.22	204.48	0.35	0.00	0.00	0.26
	$S_3^{1/3}$	7.24	21.51				
Total		119.46	225.99	0.61			
Significance		10.90	15.01				
$\mathcal{L}_{5\sigma}$ (fb $^{-1}$)		210.34	110.92				
30	$S_3^{4/3}$	20.64	19.88	0.00	0.00	0.00	1.59
	$S_3^{1/3}$	0.39	3.42				
Total		21.03	23.30	1.59			
Significance		4.42	4.67				
$\mathcal{L}_{5\sigma}$ (fb $^{-1}$)		>>10000	>>10000				

Table 27: The number of events for $2b - \text{jet} + 4 - \text{jet} + 2\mu$ final state (Equation 36) for the benchmark points and dominant SM backgrounds at a multi-TeV muon collider with the center of mass energy of 8 TeV and 30 TeV at an integrated luminosity of 1000 fb^{-1} and 10000 fb^{-1} , respectively. The required luminosities to achieve a 5σ signal ($\mathcal{L}_{5\sigma}$) are also shown for both the cases.

At this point it is worth mentioning that the significance presented in this section are slightly smaller than those quoted in the corresponding tables in previous sections, as we separate out the contributions arising from different production modes and then except the desired signal channel we treat the rest of the signal numbers as background events.

7.1 Discussion on S_1

Compiling the results for various different final states of S_1 leptoquark at the LHC, discussed in section 3, as a first step, we note down the variations of different production cross-sections and branching fractions as functions of three parameters, namely, M_{S_1} , $Y_{S_1}^{33}$ and $Z_{S_1}^{23}$. Then we weigh the signals and model backgrounds presented in any table accordingly to calculate the signal significance for different values of these three NP parameters. In this case, we find from the results quoted in subsection 3.2, which aim at the final state composed of a b -jet and τ -jet, the signal numbers in Table 4 and Table 6 are dominated by one particular production channel $c/t - g \rightarrow S_1\tau$ and $b - g \rightarrow S_1\nu$, respectively. However, the situation with final state consisting of a c -jet and τ -jet(s) (discussed in subsection 3.3) is different as in most of the cases all the production channels contribute equally and it is not possible to separate out any particular contribution with reasonable signal significance. Thus, we examine the cases described in Table 4 and Table 6 in the subsequent paragraphs.

The final state mentioned in Table 4 is $1b - \text{jet} + 1\tau - \text{jet} + 1\ell + \cancel{p}_T$, for which the $c/t - g \rightarrow S_1\tau$ acts as signal and $b - g \rightarrow S_1\nu$ serves as model background. While, the S_1 production through $c - g$ fusion depends on $Z_{S_1}^{23}$, the other two production modes involve $Y_{S_1}^{33}$ only. Now as the decay vertex of S_1 for this final state (i.e. $S_1 \rightarrow t\tau$) contains $Y_{S_1}^{33}$ alone, the total rate depends on both

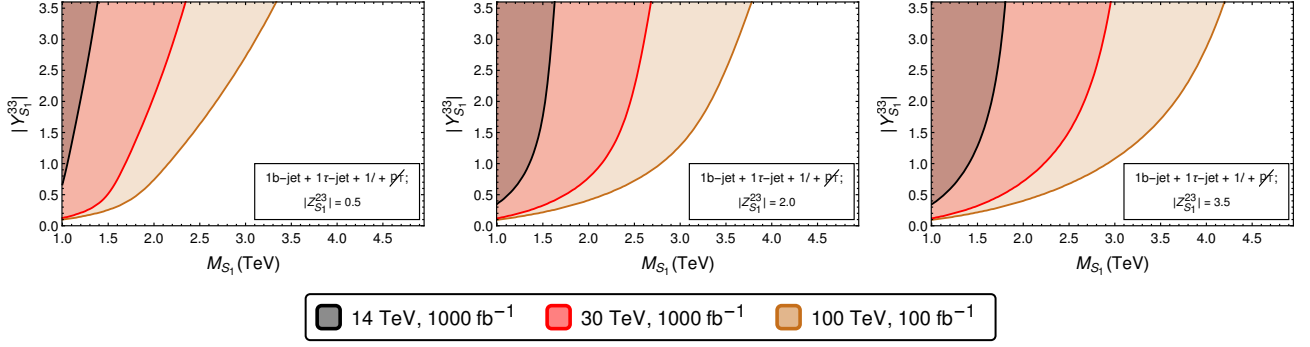


Figure 15: The regions with more than 5σ signal significance in $M_{S_1} - |Y_{S_1}^{33}|$ plane for the final state $1b - \text{jet} + 1\tau - \text{jet} + 1/\ell + \cancel{p}_T$ (see Table 4) at different center of mass energies at the LHC/FCC. The three different plots (from left) correspond to $|Z_{S_1}^{23}|$ values equal to 0.5, 2.0 and 3.5, respectively. The yellow curve represents the reach for 5σ signal significance at 100 TeV center of mass energy with 100 fb^{-1} of integrated luminosity. The red and black curves highlight the same signal significance at 30 TeV and 14 TeV center of mass energies, respectively, with 1000 fb^{-1} of integrated luminosity.

$Y_{S_1}^{33}$ and $Z_{S_1}^{23}$ couplings. The combined effects of all these facts are displayed in Figure 15 in the $M_{S_1} - |Y_{S_1}^{33}|$ plane, where the three sub-figures represent three different values of the coupling $|Z_{S_1}^{23}|$ i.e., 0.5, 2.0 and 3.5, respectively. In each plot the yellow region indicates more than 5σ signal significance with 100 TeV center of mass energies and 100 fb^{-1} integrated luminosity, whereas the red and grey regions depict the same significance at 30 TeV and 14 TeV collisions, respectively, with an integrated luminosity of 1000 fb^{-1} . Now, it is easy to understand that increasing the mass of leptoquark will decrease the signal events requiring larger values for $|Y_{S_1}^{33}|$ to reach the same significance. An interesting point to note here that each of the black, red and yellow curves gradually move toward the right side with enhancement in $|Z_{S_1}^{23}|$ value indicating that with higher value of $|Z_{S_1}^{23}|$, one needs smaller $|Y_{S_1}^{33}|$ coupling to reach the same significance for any particular mass of the leptoquark. This is due to the fact that higher $|Z_{S_1}^{23}|$ value increases the production cross-section for the signal via $c - g$ fusion while the model background, arising from the other production channels, being independent of $Z_{S_1}^{23}$ remains unaltered. We find that the 14 TeV results can probe $Y_{S_1}^{33} \sim 1$ for low leptoquark mass that is close to 1 TeV–1.5 TeV (depending on the $Z_{S_1}^{23}$ value) for this final state. However, the 30 TeV and 100 TeV searches can reach up to a 3 TeV mass for S_1 when both the couplings are at $\mathcal{O}(1)$.

The next final state we consider to explore the reaches of S_1 at the LHC/FCC is $1b - \text{jet} + \cancel{p}_T$, corresponding to the results shown in Table 6. In this case $b - g \rightarrow S_1 \nu$ process provides the signal, whereas, events from $c/t - g \rightarrow S_1 \tau$ act as model background. Therefore, the production vertex for signal as well as the decay vertex of S_1 depend only on one coupling $Y_{S_1}^{33}$, while the model background channels involve both $Y_{S_1}^{33}$ and $Z_{S_1}^{23}$. The 5σ reach of signal significance for this final state for three different $|Z_{S_1}^{23}|$ values equal to 0.5, 2.0 and 3.5 are presented in Figure 16 in three different panels, respectively. The color codes are the same as of Figure 15. In this case, unlike the previous scenario, we notice that the black, red and yellow curves shift upwards as we look at the three plots from left to right indicating necessity of higher $|Y_{S_1}^{33}|$ values with the increase in $|Z_{S_1}^{23}|$ coupling to maintain the same significance for any particular mass of the

leptoquark. The reason behind this is that the cross-section for model background from $c - g$ fusion is enhanced with the increase in $|Z_{S_1}^{23}|$ value while the signal events remain unaffected. For $|Z_{S_1}^{23}| \leq 1$, we find that this final state can probe $Y_{S_1}^{33} \sim 1$ when the leptoquark mass is around 1 TeV scale at the 14 TeV LHC, and can go up to a 2 TeV mass with higher center of mass energies like 30 TeV and 100 TeV collisions.

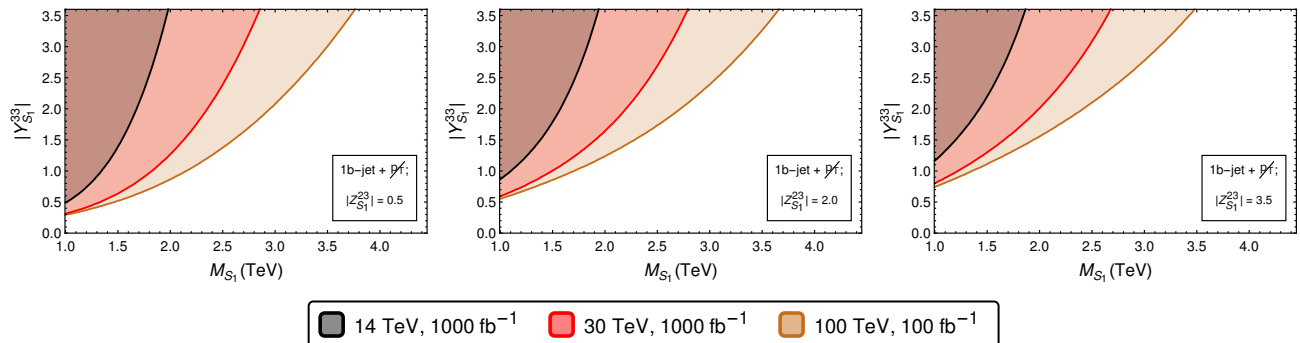


Figure 16: The regions with more than 5σ signal significance in $M_{S_1} - |Y_{S_1}^{33}|$ plane for the final state $1b - \text{jet} + \cancel{p}_T$ (see Table 6) at different center of mass energies at the LHC/FCC. The three different plots (from left) correspond to $|Z_{S_1}^{23}|$ values equal to 0.5, 2.0 and 3.5, respectively. The yellow curve represents the reach for 5σ signal significance at 100 TeV center of mass energy with 100 fb^{-1} of integrated luminosity. The red and black curves highlight the same signal significance at 30 TeV and 14 TeV center of mass energies, respectively, with 1000 fb^{-1} of integrated luminosity.

7.2 Discussion on S_3

We learn from the phenomenological study performed in section 4, section 5 and section 6 that the leptoquark S_3 is quite interesting as various different components of it give rise to quite unique signatures at colliders. The circumstance to discriminate these components becomes easier when we look for the analysis performed with BP1 and BP2 at the LHC/FCC. As the production cross-section is low in the case of BP3, we have obtained lower signal significance for it compared to the other two scenarios (BP1 and BP2), and thus is not a very favorable case to study the reach at the colliders. In subsequent subsections, we discuss the outcomes both at hadron and muon colliders separately.

7.2.1 For the LHC/FCC

It can be noted from Table 1 that in the case of BP1 and BP2, as $Y_{S_3}^{32}$ is very tiny, the phenomenology is mainly determined by the coupling $Y_{S_3}^{22}$. This simplifies the situation due to the fact that as long as $|Y_{S_3}^{22}|$ is greater than 0.03 (10 times larger than $Y_{S_3}^{32}$), the effect of $Y_{S_3}^{32}$ is insignificant. That means keeping all the other parameters unchanged, the branching fractions for different components of S_3 remain almost unaltered. Therefore, ignoring the effects of tiny $Y_{S_3}^{32}$, we adopt $|Y_{S_3}^{22}| \geq 0.03$, and hence, we are left with only two parameters in this case, which are M_{S_3} and $Y_{S_3}^{22}$.

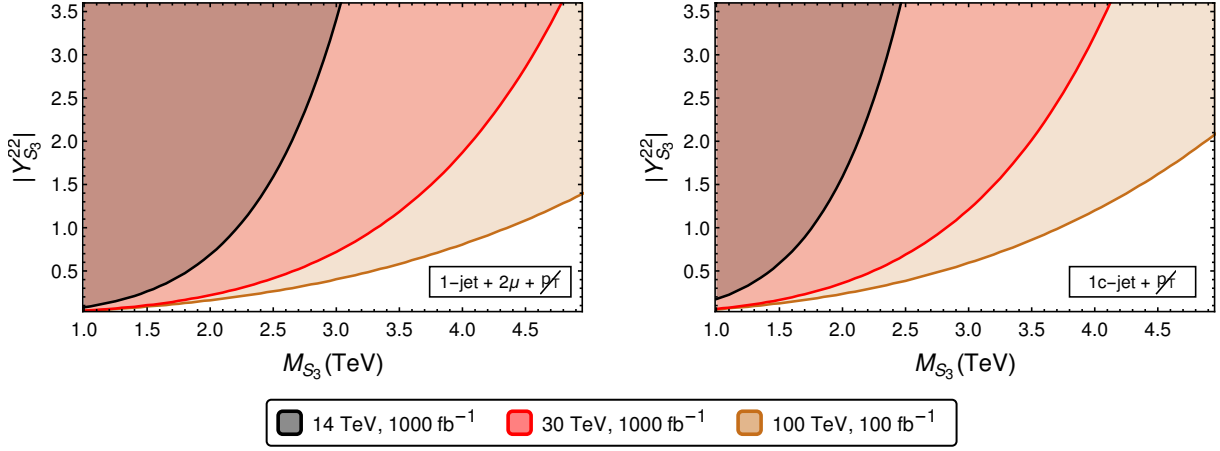


Figure 17: The regions with more than 5σ signal significance in $M_{S_3} - |Y_{S_3}^{22}|$ plane for the final states $1 - \text{jet} + 2\mu + \cancel{p}_T$ (in left panel) and $1c - \text{jet} + \cancel{p}_T$ (in right panel) at different center of mass energies at the LHC/FCC. The yellow curve represents the reach for 5σ signal significance at 100 TeV center of mass energy with 100 fb^{-1} of integrated luminosity. The red and black curves highlight the same signal significance at 30 TeV and 14 TeV center of mass energies, respectively, with 1000 fb^{-1} of integrated luminosity. The signal and SM background numbers for these two final states are highlighted in Table 15 and Table 16, respectively.

Now we first consider the two final states $1 - \text{jet} + 2\mu + \cancel{p}_T$ and $1c - \text{jet} + \cancel{p}_T$, tabulated in Table 15 and Table 16, respectively. For the first one, the signal events emerge from $sg \rightarrow S_3^{4/3} \mu$ mode and the model background comes from $cg \rightarrow S_3^{1/3} \mu$ channel making this final state a unique signature for the $S_3^{4/3}$ component. The second case corresponds to the signature for $S_3^{2/3}$ where the signal events arise from $cg \rightarrow S_3^{2/3} \nu$ mode, while the model background appears from $sg \rightarrow S_3^{1/3} \nu$ channel. The 5σ reach for these two final states with varying M_{S_3} and $Y_{S_3}^{22}$ are presented in the left and right panels of Figure 17, respectively. The yellow region signifies signal significance of more than 5σ at 100 TeV center of mass energy with 100 fb^{-1} integrated luminosity, and the respective red and the grey region indicate the same significance at the 30 TeV and 14 TeV center of mass energies with 1000 fb^{-1} of luminosity. It can be seen that the final state $1 - \text{jet} + 2\mu + \cancel{p}_T$ probes larger parameter space than the final state $1c - \text{jet} + \cancel{p}_T$ as higher significance can be attained with the former one for same values of M_{S_3} and $Y_{S_3}^{22}$. We find that the 14 TeV results for $1 - \text{jet} + 2\mu + \cancel{p}_T$ is quite promising as it can probe $Y_{S_3}^{22} \sim 1$ until 2 TeV mass of the leptoquark S_3 and with higher center of mass energies like 30 TeV and 100 TeV, the same coupling value can be probed until more than 3 TeV and 4 TeV mass of S_3 , respectively. In the case of $1c - \text{jet} + \cancel{p}_T$ final state, with $Y_{S_3}^{22} \sim 1$, the mass reach for S_3 for the three center of mass energies 14 TeV, 30 TeV and 100 TeV are 1.7 TeV, 2.8 TeV and 3.6 TeV, respectively. It is worthwhile to point out that both these two channels have much higher reach in the S_3 mass axis compared to the cases discussed in the previous subsection (subsection 7.1) for S_1 leptoquark for an $\mathcal{O}(1)$ value of the corresponding Yukawa type coupling(s).

Having discussed the status of the two components of S_3 , namely, $S_3^{4/3}$ and $S_3^{1/3}$, we now focus on the final states corresponding to $S_3^{1/3}$ component. For this purpose we select the two following decay topologies: $1c - \text{jet} + 2\mu + \cancel{p}_T$ (see Table 17) and $1c - \text{jet} + 1\mu + \cancel{p}_T$ (see Table 18). The final

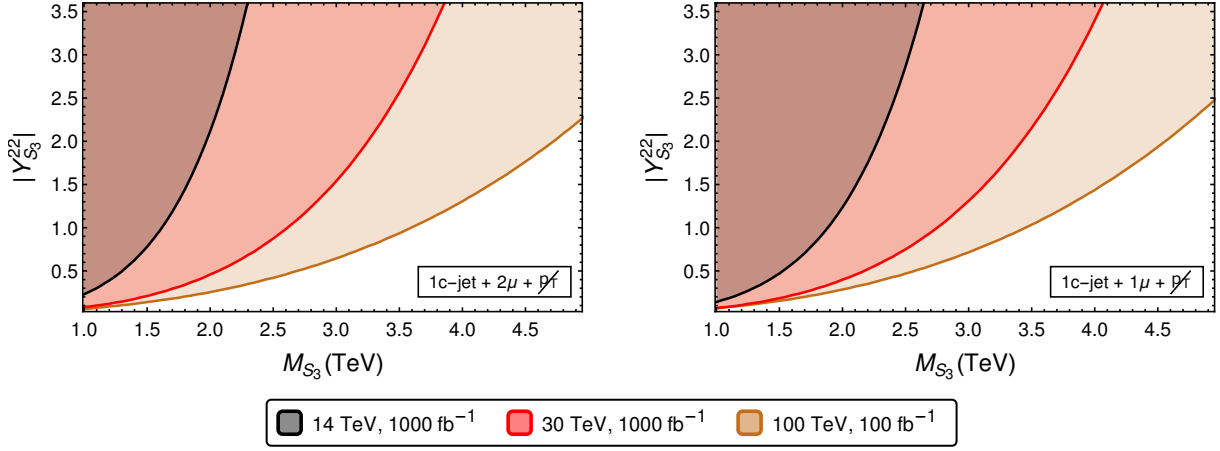


Figure 18: The regions with more than 5σ signal significance in $M_{S_3} - |Y_{S_3}^{22}|$ plane for the final states $1c - \text{jet} + 2\mu + \cancel{p}_T$ (in left panel) and $1c - \text{jet} + 1\mu + \cancel{p}_T$ (in right panel) at different center of mass energies at the LHC/FCC. The yellow curve represents the reach for 5σ signal significance at 100 TeV center of mass energy with 100 fb^{-1} of integrated luminosity. The red and black curves highlight the same signal significance at 30 TeV and 14 TeV center of mass energies, respectively, with 1000 fb^{-1} of integrated luminosity. The signal and SM background numbers for these two final states are highlighted in Table 17 and Table 18, respectively.

state $1c - \text{jet} + 2\mu + \cancel{p}_T$ mainly arises from the channel $cg \rightarrow S_3^{1/3}\mu$ where the mode $sg \rightarrow S_3^{4/3}\mu$ acts as model background. Likewise, the final state $1c - \text{jet} + 1\mu + \cancel{p}_T$ is generated from the production channel $sg \rightarrow S_3^{1/3}\nu$ whereas the modes $sg \rightarrow S_3^{4/3}\mu$ and $cg \rightarrow S_3^{1/3}\mu$ function as model backgrounds. The left and right panels of Figure 18 illustrate the 5σ reach for these two final states, respectively, at three different center of mass energies and the similar luminosity choices as described in the last paragraphs. We can see from the left panel of Figure 18 that the presence of c -jet in the final state reduces the signal significance compared to the left panel of Figure 17 that has a similar final state except for a replacement of the c -jet with a light-jet. This is due to the fact that we have an enhancement factor for the $S_3^{1/3}$ channel (i.e., $1 - \text{jet} + 2\mu + \cancel{p}_T$) arising from the interaction vertex and also a suppression factor in $1c - \text{jet} + 2\mu + \cancel{p}_T$ originating from the branching fraction of $S_3^{1/3}$. The right panel of Figure 18 provides cheering situation where for $Y_{S_3}^{22} \sim 1$, we can probe the leptoquark mass up to the 1.8 TeV, 2.7 TeV and 3.5 TeV scale with the 14 TeV, 30 TeV and 100 TeV collisions, respectively.

7.2.2 For a muon collider

We continue to explore the similar outcomes at a multi-TeV muon collider. Here, the most encouraging final state is $2 - \text{jet} + 2\mu$ (see Table 24) where we find enormously healthy signal numbers that arise from the $S_3^{4/3}$ component of S_3 , rendering a huge significance for such a signal. Thus one can achieve the 5σ signal significance with very small value of $|Y_{S_3}^{22}|$ coupling and for large mass of the S_3 leptoquark. A similar scenario occurs for $2b - \text{jet} + 2\mu$ final state in BP3 too. Therefore, we focus on $2c - \text{jet} + 2\mu$ final state in BP1 scenario. As already shown in Table 25, $S_3^{1/3}$ provides signal events for this final state while $S_3^{4/3}$ behaves as a model background. The 5σ reach plot, in the $M_{S_3} - |Y_{S_3}^{22}|$ plane, for this final state is depicted in Figure 19. The yellow region

signifies the parameter space with signal significance of more than 5σ level with the center of mass energy being 30 TeV and an integrated luminosity of 10000 fb^{-1} , whereas the same signal significance with 8 TeV center of mass energy and 1000 fb^{-1} integrated luminosity is shown in grey. It should be kept in mind that at 8 TeV center of mass energy, leptoquark of mass greater than 4 TeV can not be produced in pairs. Therefore, we find a sharp rise of the black curve while approaching the mass of 4 TeV indicating no sensitivity after that mass scale. On the other hand, the 5σ reach for 30 TeV energy with an integrated luminosity of 10000 fb^{-1} (shown by the yellow curve) remains almost flat for the small value of $|Y_{S_3}^{22}|$ until very large mass of the leptoquark. It is apparent from the discussions that the muon collider has much more sensitivity to probe the small coupling values up to the very large mass of the leptoquark compared to the hadron collider.

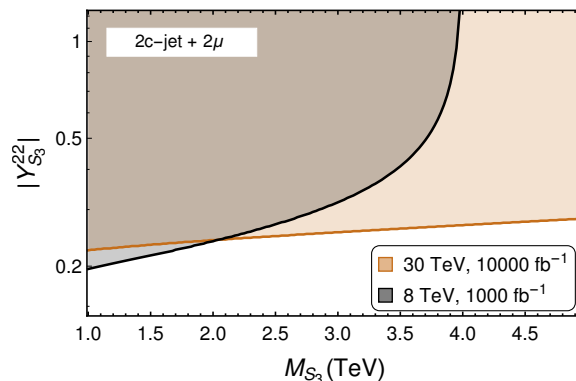


Figure 19: The regions with more than 5σ significance in $M_{S_3} - |Y_{S_3}^{22}|$ plane for the final state $2c - \text{jet} + 2\mu$ (see Table 25) at two different center of mass energies at a multi-TeV muon collider. The yellow (black) curve represents the reach for 5σ signal significance at 30 TeV (8 TeV) center of mass energy with 10000 fb^{-1} (1000 fb^{-1}) integrated luminosity.

8 Conclusion

In this article we study the phenomenology of two scalar leptoquarks via single production channels mediated by quark gluon fusions. The leptoquarks carry color as well as electromagnetic charge, while the leptoquark S_1 is singlet and S_3 is triplet under the weak gauge group. The decays of these leptoquarks are dictated by specific non-vanishing couplings to fermions where the choice is governed by the series of discrepancies observed in B -decays. However, we have demonstrated that our analysis is general enough and can easily be adopted to any scenario for the collider searches.

The pair productions of the leptoquarks at hadron collider are mostly dominated via QCD processes like gluon fusions, however, the single leptoquark productions which can probe the Yukawa-type couplings of the leptoquark to a quark and a lepton become efficient at high energies. The current and upcoming searches at the LHC/FCC plays the key role here. Whereas, interestingly a multi-TeV muon collider can be effective in probing these same Yukawa-type couplings through pair productions of the leptoquarks. We first consider different final states bearing distinguishable signatures arising from the S_1 leptoquark and three different components

of the S_3 leptoquark. In case of a TeV mass range S_1 , we find among several decay topologies, $1b - \text{jet} + 1\tau - \text{jet} + 1\ell + \cancel{p}_T$ and $1b + \cancel{p}_T$ are the most promising ones which can probe the Yukawa-type coupling $Y_{S_1}^{33}$ as low as 0.1 and 0.3, respectively, for $Z_{S_1}^{23} \leq 0.5$ at the LHC/FCC with upgraded luminosity. Next we have illustrated that when S_1 is produced in association with a visible particle (say a charged lepton), the further decay $S_1 \rightarrow \bar{c}\tau^+ \rightarrow \bar{c}\pi^+\bar{\nu}$ leads to invariant mass edge at the S_1 mass, which can be instrumental in determination of the leptoquark mass scale at the LHC.

The phenomenology is richer in the case of S_3 leptoquark where three different components, namely $S_3^{4/3}$, $S_3^{2/3}$ and $S_3^{1/3}$ are produced with the same tree-level mass. For our choices of the benchmark points these components often decays into final states consisting of muons compared to tau leptons as observed in the case of S_1 . We notice that $S_3^{4/3}$ and $S_3^{2/3}$ components have distinctive signatures; $1 - \text{jet} + 2\mu + \cancel{p}_T \leq 30 \text{ GeV}$ and $1c - \text{jet} + \cancel{p}_T \geq 500 \text{ GeV}$, respectively, which can probe very low values ($\lesssim \mathcal{O}(10^{-1})$) of the Yukawa-type coupling $Y_{S_3}^{22}$ for a TeV mass scale S_3 at the upcoming upgrades of the LHC. On the other hand $S_3^{1/3}$ has four modes to search for, and focusing on the most encouraging ones $2\mu + 1c - \text{jet} + \cancel{p}_T \leq 30 \text{ GeV}$ and $1\mu + 1c - \text{jet} + \cancel{p}_T \geq 200 \text{ GeV}$, we find a similar small values of $Y_{S_3}^{22}$ can be explored at the LHC/FCC. Additionally, we also briefed about the lepton flavor violating signatures in the decay caused due to the off-diagonal Yukawa-type coupling $Y_{S_3}^{32}$. In all cases, the event and the SM background numbers are presented at the LHC/FCC for three with center of mass energies 14 TeV, 30 TeV and 100 TeV which exhibit a maximum reach of around 4 TeV mass for S_1 and more than 5 TeV mass for the S_3 leptoquark.

We also explore the possibilities for direct searches of leptoquarks at a multi-TeV muon collider considering two different center of mass energies namely, 8 TeV and 30 TeV. Here in most cases, we rely on the pair productions via t -channel processes (through quarks) to probe the relevant Yukawa-type couplings, except for the $S_3^{2/3}$ component of S_3 which can only be produced via s -channel exchange of photon and Z -boson. The situation for S_1 leptoquark is very similar to that of $S_3^{2/3}$ component, as S_1 does not couple to muon for the chosen benchmark scenarios and thus can only be produced through the mentioned s -channel processes. Therefore, with the main intention to probe the Yukawa-type couplings of the leptoquarks, we analyze the pair productions of $S_3^{4/3}$ and $S_3^{1/3}$ components via t -channel contributions. The distinctive feature of these two components are found to be prominent here as well. For $S_3^{4/3}$, the final state consisting of $2 - \text{jet} + 2\mu$ (for BP1) and $2b - \text{jet} + 2\mu$ (for BP3) can probe the $Y_{S_3}^{22}$ coupling up to its perturbativity limit for $\mathcal{O}(10 \text{ TeV})$ mass leptoquark with a very early data at muon collider. The reach calculated for the topology $2c + 2\mu$ shows a lower sensitivity of $Y_{S_3}^{22} \sim 0.2$. To conclude, we find that the prospect of the scalar leptoquarks and their different $SU(2)_L$ components can be distinguished and segregated with the complementarity of hadron and muon colliders.

Acknowledgments

The authors thank Rahul Sinha for useful suggestions. P.B. and A.K. acknowledge SERB CORE Grant CRG/2018/004971 and MATRICS Grant MTR/2020/000668 for the financial support. The work of R.M. is partly supported by the Alexander von Humboldt Foundation and the University of Siegen under the Young Investigator Research Group (Nachwuchsforscherinnengruppe) grant.

References

- [1] H. Georgi and S. Glashow, *Unity of All Elementary Particle Forces*, *Phys. Rev. Lett.* **32** (1974) 438–441.
- [2] J. C. Pati and A. Salam, *Lepton Number as the Fourth Color*, *Phys. Rev. D* **10** (1974) 275–289. [Erratum: *Phys. Rev. D* 11, 703–703 (1975)].
- [3] LHCb collaboration, R. Aaij et al., *Search for lepton-universality violation in $B^+ \rightarrow K^+ \ell^+ \ell^-$ decays*, *Phys. Rev. Lett.* **122** (2019) 191801, [[1903.09252](#)].
- [4] LHCb collaboration, R. Aaij et al., *Test of lepton universality in beauty-quark decays*, [2103.11769](#).
- [5] LHCb collaboration, R. Aaij et al., *Test of lepton universality with $B^0 \rightarrow K^{*0} \ell^+ \ell^-$ decays*, *JHEP* **08** (2017) 055, [[1705.05802](#)].
- [6] LHCb collaboration, R. Aaij et al., *Branching fraction measurements of the rare $B_s^0 \rightarrow \phi \mu^+ \mu^-$ and $B_s^0 \rightarrow f_2'(1525) \mu^+ \mu^-$ decays*, [2105.14007](#).
- [7] LHCb collaboration, R. Aaij et al., *Measurement of CP-Averaged Observables in the $B^0 \rightarrow K^{*0} \mu^+ \mu^-$ Decay*, *Phys. Rev. Lett.* **125** (2020) 011802, [[2003.04831](#)].
- [8] HFLAV collaboration, Y. S. Amhis et al., *Averages of b-hadron, c-hadron, and τ -lepton properties as of 2018*, *Eur. Phys. J. C* **81** (2021) 226, [[1909.12524](#)].
- [9] J. Blumlein, E. Boos and A. Kryukov, *Leptoquark pair production in hadronic interactions*, *Z. Phys. C* **76** (1997) 137–153, [[hep-ph/9610408](#)].
- [10] A. Belyaev, C. Leroy, R. Mehdiyev and A. Pukhov, *Leptoquark single and pair production at LHC with CalcHEP/CompHEP in the complete model*, *JHEP* **09** (2005) 005, [[hep-ph/0502067](#)].
- [11] M. Kramer, T. Plehn, M. Spira and P. Zerwas, *Pair production of scalar leptoquarks at the Tevatron*, *Phys. Rev. Lett.* **79** (1997) 341–344, [[hep-ph/9704322](#)].
- [12] T. Plehn, H. Spiesberger, M. Spira and P. Zerwas, *Formation and decay of scalar leptoquarks/squarks in ep collisions*, *Z. Phys. C* **74** (1997) 611–614, [[hep-ph/9703433](#)].
- [13] O. J. P. Eboli, R. Zukanovich Funchal and T. L. Lungov, *Signal and backgrounds for leptoquarks at the CERN LHC*, *Phys. Rev. D* **57** (1998) 1715–1729, [[hep-ph/9709319](#)].
- [14] M. Kramer, T. Plehn, M. Spira and P. M. Zerwas, *Pair production of scalar leptoquarks at the CERN LHC*, *Phys. Rev. D* **71** (2005) 057503, [[hep-ph/0411038](#)].
- [15] J. B. Hammett and D. A. Ross, *NLO Leptoquark Production and Decay: The Narrow-Width Approximation and Beyond*, *JHEP* **07** (2015) 148, [[1501.06719](#)].
- [16] T. Mandal, S. Mitra and S. Seth, *Single Productions of Colored Particles at the LHC: An Example with Scalar Leptoquarks*, *JHEP* **07** (2015) 028, [[1503.04689](#)].

- [17] K. S. Babu, P. S. B. Dev, S. Jana and A. Thapa, *Unified framework for B -anomalies, muon $g - 2$ and neutrino masses*, *JHEP* **03** (2021) 179, [[2009.01771](#)].
- [18] D. Marzocca, *Addressing the B -physics anomalies in a fundamental Composite Higgs Model*, *JHEP* **07** (2018) 121, [[1803.10972](#)].
- [19] S. Saad, *Combined explanations of $(g - 2)_\mu$, $R_{D^{(*)}}$, $R_{K^{(*)}}$ anomalies in a two-loop radiative neutrino mass model*, *Phys. Rev. D* **102** (2020) 015019, [[2005.04352](#)].
- [20] V. Gherardi, D. Marzocca and E. Venturini, *Low-energy phenomenology of scalar leptoquarks at one-loop accuracy*, *JHEP* **01** (2021) 138, [[2008.09548](#)].
- [21] D. Bečirević, I. Doršner, S. Fajfer, N. Košnik, D. A. Faroughy and O. Sumensari, *Scalar leptoquarks from grand unified theories to accommodate the B -physics anomalies*, *Phys. Rev. D* **98** (2018) 055003, [[1806.05689](#)].
- [22] I. Bigaran, J. Gargalionis and R. R. Volkas, *A near-minimal leptoquark model for reconciling flavour anomalies and generating radiative neutrino masses*, *JHEP* **10** (2019) 106, [[1906.01870](#)].
- [23] A. Crivellin, D. Müller and F. Saturnino, *Flavor Phenomenology of the Leptoquark Singlet-Triplet Model*, *JHEP* **06** (2020) 020, [[1912.04224](#)].
- [24] A. Crivellin, D. Müller and T. Ota, *Simultaneous explanation of $R(D^{(*)})$ and $b \rightarrow s\mu^+\mu^-$: the last scalar leptoquarks standing*, *JHEP* **09** (2017) 040, [[1703.09226](#)].
- [25] U. Aydemir, T. Mandal and S. Mitra, *Addressing the $\mathbf{R}_{D^{(*)}}$ anomalies with an \mathbf{S}_1 leptoquark from $\mathbf{SO}(10)$ grand unification*, *Phys. Rev. D* **101** (2020) 015011, [[1902.08108](#)].
- [26] T. Mandal, S. Mitra and S. Raz, *$R_{D^{(*)}}$ motivated \mathbf{S}_1 leptoquark scenarios: Impact of interference on the exclusion limits from LHC data*, *Phys. Rev. D* **99** (2019) 055028, [[1811.03561](#)].
- [27] S. Iguro, M. Takeuchi and R. Watanabe, *Testing leptoquark/EFT in $\bar{B} \rightarrow D^{(*)}l\bar{\nu}$ at the LHC*, *Eur. Phys. J. C* **81** (2021) 406, [[2011.02486](#)].
- [28] H. M. Lee, *Leptoquark option for B -meson anomalies and leptonic signatures*, *Phys. Rev. D* **104** (2021) 015007, [[2104.02982](#)].
- [29] I. Doršner, S. Fajfer and A. Lejlić, *Novel Leptoquark Pair Production at LHC*, *JHEP* **05** (2021) 167, [[2103.11702](#)].
- [30] P. Bandyopadhyay and R. Mandal, *Revisiting scalar leptoquark at the LHC*, *Eur. Phys. J. C* **78** (2018) 491, [[1801.04253](#)].
- [31] A. Bhaskar, T. Mandal and S. Mitra, *Boosting vector leptoquark searches with boosted tops*, *Phys. Rev. D* **101** (2020) 115015, [[2004.01096](#)].
- [32] A. Bhaskar, D. Das, T. Mandal, S. Mitra and C. Neeraj, *Precise limits on the charge-2/3 U_1 vector leptoquark*, [2101.12069](#).

- [33] A. Bhaskar, T. Mandal, S. Mitra and M. Sharma, *Improving third-generation leptoquark searches with combined signals and boosted top*, [2106.07605](#).
- [34] L. Da Rold, M. Epele, A. Medina, N. I. Mileo and A. Szyrkman, *Enhancement of the double Higgs production via leptoquarks at the LHC*, [2105.06309](#).
- [35] G. Hiller, D. Loose and I. Nišandžić, *Flavorful leptoquarks at the LHC and beyond: spin 1*, *JHEP* **06** (2021) 080, [[2103.12724](#)].
- [36] U. Haisch and G. Polesello, *Resonant third-generation leptoquark signatures at the Large Hadron Collider*, *JHEP* **05** (2021) 057, [[2012.11474](#)].
- [37] K. Chandak, T. Mandal and S. Mitra, *Hunting for scalar leptoquarks with boosted tops and light leptons*, *Phys. Rev. D* **100** (2019) 075019, [[1907.11194](#)].
- [38] A. Bhaskar, D. Das, B. De and S. Mitra, *Enhancing scalar productions with leptoquarks at the LHC*, *Phys. Rev. D* **102** (2020) 035002, [[2002.12571](#)].
- [39] A. Alves, O. J. t. Eboli, G. Grilli Di Cortona and R. R. Moreira, *Indirect and monojet constraints on scalar leptoquarks*, *Phys. Rev. D* **99** (2019) 095005, [[1812.08632](#)].
- [40] I. Doršner, S. Fajfer and M. Patra, *A comparative study of the S_1 and U_1 leptoquark effects in the light quark regime*, *Eur. Phys. J. C* **80** (2020) 204, [[1906.05660](#)].
- [41] S. Mandal, M. Mitra and N. Sinha, *Probing leptoquarks and heavy neutrinos at the LHeC*, *Phys. Rev. D* **98** (2018) 095004, [[1807.06455](#)].
- [42] R. Padhan, S. Mandal, M. Mitra and N. Sinha, *Signatures of \tilde{R}_2 class of Leptoquarks at the upcoming ep colliders*, *Phys. Rev. D* **101** (2020) 075037, [[1912.07236](#)].
- [43] M. J. Baker, J. Fuentes-Martín, G. Isidori and M. König, *High- p_T signatures in vector-leptoquark models*, *Eur. Phys. J. C* **79** (2019) 334, [[1901.10480](#)].
- [44] H. Nadeau and D. London, *Leptoquarks at e gamma colliders*, *Phys. Rev. D* **47** (1993) 3742–3749, [[hep-ph/9303238](#)].
- [45] S. Atag and O. Cakir, *Pair production of scalar leptoquarks at TeV energy gamma p colliders*, *Phys. Rev. D* **49** (1994) 5769–5772.
- [46] S. Atag, A. Celikel and S. Sultansoy, *Scalar leptoquark production at TeV energy gamma p colliders*, *Phys. Lett. B* **326** (1994) 185–189.
- [47] W. Buchmuller, R. Ruckl and D. Wyler, *Leptoquarks in Lepton - Quark Collisions*, *Phys. Lett. B* **191** (1987) 442–448. [Erratum: *Phys.Lett.B* 448, 320–320 (1999)].
- [48] J. Hewett and T. Rizzo, *Leptoquark Signals at e^+e^- Colliders*, *Phys. Rev. D* **36** (1987) 3367.
- [49] J. Hewett and S. Pakvasa, *Leptoquark Production in Hadron Colliders*, *Phys. Rev. D* **37** (1988) 3165.

- [50] F. Cuyppers, *Leptoquark production in $e^- \gamma$ scattering*, *Nucl. Phys. B* **474** (1996) 57–71, [[hep-ph/9508397](#)].
- [51] P. Bandyopadhyay, S. Dutta and A. Karan, *Investigating the Production of Leptoquarks by Means of Zeros of Amplitude at Photon Electron Collider*, *Eur. Phys. J. C* **80** (2020) 573, [[2003.11751](#)].
- [52] P. Bandyopadhyay, S. Dutta and A. Karan, *Zeros of amplitude in the associated production of photon and leptoquark at $e - p$ collider*, *Eur. Phys. J. C* **81** (2021) 315, [[2012.13644](#)].
- [53] P. Bandyopadhyay, S. Dutta, M. Jakkapu and A. Karan, *Exploring spins of beyond Standard Models via angular distribution at the LHC*, [2007.12997](#).
- [54] S. Dutta, P. Bandyopadhyay and A. Karan, *Distinguishing Different BSM Signatures at Present and Future Colliders*, [2105.00893](#).
- [55] R. Mandal and A. Pich, *Constraints on scalar leptoquarks from lepton and kaon physics*, *JHEP* **12** (2019) 089, [[1908.11155](#)].
- [56] S. Davidson, D. C. Bailey and B. A. Campbell, *Model independent constraints on leptoquarks from rare processes*, *Z. Phys. C* **61** (1994) 613–644, [[hep-ph/9309310](#)].
- [57] I. Doršner, S. Fajfer, A. Greljo, J. Kamenik and N. Košnik, *Physics of leptoquarks in precision experiments and at particle colliders*, *Phys. Rept.* **641** (2016) 1–68, [[1603.04993](#)].
- [58] ATLAS collaboration, G. Aad et al., *Search for pairs of scalar leptoquarks decaying into quarks and electrons or muons in $\sqrt{s} = 13$ TeV pp collisions with the ATLAS detector*, *JHEP* **10** (2020) 112, [[2006.05872](#)].
- [59] CMS collaboration, A. M. Sirunyan et al., *Search for singly and pair-produced leptoquarks coupling to third-generation fermions in proton-proton collisions at $\sqrt{s} = 13$ TeV*, *Phys. Lett. B* **819** (2021) 136446, [[2012.04178](#)].
- [60] ATLAS collaboration, G. Aad et al., *Search for pair production of third-generation scalar leptoquarks decaying into a top quark and a τ -lepton in pp collisions at $\sqrt{s} = 13$ TeV with the ATLAS detector*, *JHEP* **06** (2021) 179, [[2101.11582](#)].
- [61] M. Cepeda et al., *Report from Working Group 2: Higgs Physics at the HL-LHC and HE-LHC*, *CERN Yellow Rep. Monogr.* **7** (2019) 221–584, [[1902.00134](#)].
- [62] FCC collaboration, A. Abada et al., *FCC Physics Opportunities: Future Circular Collider Conceptual Design Report Volume 1*, *Eur. Phys. J. C* **79** (2019) 474.
- [63] C. M. Ankenbrandt et al., *Status of muon collider research and development and future plans*, *Phys. Rev. ST Accel. Beams* **2** (1999) 081001, [[physics/9901022](#)].
- [64] D. Neuffer and V. Shiltsev, *On the feasibility of a pulsed 14 TeV c.m.e. muon collider in the LHC tunnel*, *JINST* **13** (2018) T10003, [[1811.10694](#)].

- [65] J. P. Delahaye, M. Diemoz, K. Long, B. Mansoulié, N. Pastrone, L. Rivkin et al., *Muon Colliders*, [1901.06150](#).
- [66] T. Han, Y. Ma and K. Xie, *Quark and Gluon Contents of a Lepton at High Energies*, [2103.09844](#).
- [67] P. Bandyopadhyay and A. Costantini, *Obscure Higgs boson at Colliders*, *Phys. Rev. D* **103** (2021) 015025, [[2010.02597](#)].
- [68] G.-y. Huang, F. S. Queiroz and W. Rodejohann, *Gauged $L_\mu-L_\tau$ at a muon collider*, *Phys. Rev. D* **103** (2021) 095005, [[2101.04956](#)].
- [69] C. Sen, P. Bandyopadhyay, S. Dutta and A. KT, *Displaced Higgs production in Type-III Seesaw at the LHC/FCC, MATHUSLA and Muon collider*, [2107.12442](#).
- [70] A. Costantini, F. De Lillo, F. Maltoni, L. Mantani, O. Mattelaer, R. Ruiz et al., *Vector boson fusion at multi-TeV muon colliders*, *JHEP* **09** (2020) 080, [[2005.10289](#)].
- [71] G.-Y. Huang, S. Jana, F. S. Queiroz and W. Rodejohann, *Probing the $R_{K^{(*)}}$ Anomaly at a Muon Collider*, [2103.01617](#).
- [72] P. Asadi, R. Capdevilla, C. Cesarotti and S. Homiller, *Searching for Leptoquarks at Future Muon Colliders*, [2104.05720](#).
- [73] N. Cabibbo, *Unitary Symmetry and Leptonic Decays*, *Phys. Rev. Lett.* **10** (1963) 531–533.
- [74] M. Kobayashi and T. Maskawa, *CP Violation in the Renormalizable Theory of Weak Interaction*, *Prog. Theor. Phys.* **49** (1973) 652–657.
- [75] R. Mandal, C. Murgui, A. Peñuelas and A. Pich, *The role of right-handed neutrinos in $b \rightarrow c\tau\bar{\nu}$ anomalies*, *JHEP* **08** (2020) 022, [[2004.06726](#)].
- [76] P. Arnan, D. Becirevic, F. Mescia and O. Sumensari, *Probing low energy scalar leptoquarks by the leptonic W and Z couplings*, *JHEP* **02** (2019) 109, [[1901.06315](#)].
- [77] A. Falkowski and D. Straub, *Flavourful SMEFT likelihood for Higgs and electroweak data*, *JHEP* **04** (2020) 066, [[1911.07866](#)].
- [78] L. Di Luzio, M. Kirk, A. Lenz and T. Rauh, *ΔM_s theory precision confronts flavour anomalies*, *JHEP* **12** (2019) 009, [[1909.11087](#)].
- [79] W. Altmannshofer and P. Stangl, *New Physics in Rare B Decays after Moriond 2021*, [2103.13370](#).
- [80] F. Staub, *SARAH 4 : A tool for (not only SUSY) model builders*, *Comput. Phys. Commun.* **185** (2014) 1773–1790, [[1309.7223](#)].
- [81] A. Belyaev, N. D. Christensen and A. Pukhov, *CalcHEP 3.4 for collider physics within and beyond the Standard Model*, *Comput. Phys. Commun.* **184** (2013) 1729–1769, [[1207.6082](#)].

- [82] T. Sjostrand, S. Mrenna and P. Z. Skands, *PYTHIA 6.4 Physics and Manual*, *JHEP* **05** (2006) 026, [[hep-ph/0603175](#)].
- [83] M. Cacciari, G. P. Salam and G. Soyez, *FastJet User Manual*, *Eur. Phys. J. C* **72** (2012) 1896, [[1111.6097](#)].
- [84] NNPDF collaboration, E. R. Nocera, R. D. Ball, S. Forte, G. Ridolfi and J. Rojo, *A first unbiased global determination of polarized PDFs and their uncertainties*, *Nucl. Phys. B* **887** (2014) 276–308, [[1406.5539](#)].
- [85] CMS collaboration, A. M. Sirunyan et al., *Identification of heavy-flavour jets with the CMS detector in pp collisions at 13 TeV*, *JINST* **13** (2018) P05011, [[1712.07158](#)].
- [86] CMS collaboration, I. R. Tomalin, *b tagging in CMS*, *J. Phys. Conf. Ser.* **110** (2008) 092033.
- [87] CMS collaboration, *B -tagging performance of the CMS Legacy dataset 2018*, *TWiki @ CERN*.
- [88] G. Bagliesi, *Tau tagging at Atlas and CMS*, in *17th Symposium on Hadron Collider Physics 2006 (HCP 2006)*, [0707.0928](#).
- [89] CMS collaboration, G. L. Bayatian et al., *CMS technical design report, volume II: Physics performance*, *J. Phys. G* **34** (2007) 995–1579.
- [90] ATLAS collaboration, *Performance and Calibration of the JetFitterCharm Algorithm for c -Jet Identification*, *ATL-PHYS-PUB-2015-001*.
- [91] N. Mohr, *Dilepton mass edge measurement in SUSY events with CMS*, in *44th Rencontres de Moriond on Electroweak Interactions and Unified Theories*, [0904.3408](#).
- [92] CMS collaboration, *Discovery potential and measurement of a dilepton mass edge in SUSY events at $\sqrt{s} = 10$ TeV*, *CMS-PAS-SUS-09-002*.
- [93] H. Al Ali et al., *The Muon Smasher’s Guide*, [2103.14043](#).